ROS-scavenging-associated transcriptional and biochemical shifts during nectarine fruit development and ripening

Núria Vall-llaura[1,#], Pablo Fernández-Cancelo[1,#], Isabel Nativitas-Lima[1,2], Gemma Echeverria[1], Neus Teixidó[1], Christian Larrigaudière[1], Rosario Torres[1] and Jordi Giné-Bordonaba[1,*]

[1]*IRTA, Postharvest Programme, Edifici Fruitcentre, Parc Científic i Tecnològic Agroalimentari de Lleida, Parc de Gardeny, 25003 Lleida, Catalonia, Spain.*

[2]*Colegio de Postgraduados (COLPOS), Campus Montecillo, 56230, Texcoco, México*

[#]*Both authors contributed equally to this manuscript*

***Corresponding Author:** Jordi Giné-Bordonaba (jordi.gine@irta.cat)

Official email addresses of all authors: Núria Vall-llaura (nuria.vall-llaura@irta.cat), Pablo Fernández-Cancelo (pablo.fernandez@irta.cat), Isabel Nativitas (nativitas.isabel@colpos.mx)**,** Gemma Echeverria (gemma.echeverria@irta.cat), Neus Teixidó (neus.teixido@irta.cat), Christian Larrigaudière (christian.larrigaudiere@irta.cat), Rosario Torres (rosario.torres@irta.cat) and Jordi Giné-Bordonaba (jordi.gine@irta.cat).

Abstract

ROS are known as toxic by-products but also as important signaling molecules playing a key role in fruit development and ripening. To counteract the negative effects of ROS, plants and fruit own multiple ROS-scavenging mechanisms aiming to ensure a balanced ROS homeostasis. In the present study, changes in specific ROS (i.e. H_2O_2) as well as enzymatic (SOD, CAT, POX, APX) and non-enzymatic (phenylpropanoids, carotenoids and ascorbate) ROS-scavenging systems were investigated along four different stages of nectarine (cv. 'Diamond Ray') fruit development and ripening (39, 70, 94 and 121 DAFB) both at the metabolic (28 individual metabolites or enzymes) and transcriptional level (24 genes). Overall, our results demonstrate a complex ROS-related transcriptome and metabolome reprogramming during fruit development and ripening. At earlier fruit developmental stages an increase on the respiration rate is likely triggering an oxidative burst and resulting in the activation of specific ethylene response factors (*ERF1*). In turn, ROS-responsive genes or the biosynthesis of specific antioxidant compounds (i.e. phenylpropanoids) were highly expressed or accumulated at earlier fruit developmental stages (39-70 DAFB). Nonetheless, as the fruit develops, the decrease in the fruit respiration rate and the reduction of *ERF1* genes leads to lower levels of most non-enzymatic antioxidants and higher accumulation of H_2O_2. Based on available literature and the observed accumulation dynamics of H_2O_2, it is anticipated that this compound may not only be a by-product of ROS-scavenging but also a signaling molecule accumulated during the ripening of nectarine fruit.

Keywords: Antioxidant enzymes, carotenoids, ethylene, ERF, phenolic compounds, respiration.

1. Introduction

Fruit development and ripening are coordinated physiological events controlled by hormonal and epigenetic regulation and ultimately tuned by environmental cues (Palma et al., 2019). In the specific case of *Prunus persica*, fruit development from pollination to fully ripe fruit may take from 90 to 160 days, depending on the cultivar and the fruit harvest season (Reig et al., 2013). Peach growth generally shows a double sigmoid curve with up to four differentiated phases (Tonutti et al., 1991). Among those, fruit development mainly occurs during three of them and the lag interval between stages is referred as the stone formation. Nectarine ripening understood as changes in skin colour, softening and flavour development mainly occurs during the last developmental phase (Zhang and Jia, 2005) driven by the action of the hormone ethylene (Hayama et al., 2006). Nonetheless, multiple studies suggest that additional compounds including other hormones (Soto et al., 2013), reactive oxygen species (ROS), or even specific compounds, i.e. sucrose (Jia et al., 2016) or carotenoids (Diretto et al., 2020), can regulate fruit ripening in other species.

In fact, fruit development and ripening are accompanied by multiple oxidative events leading to ROS accumulation, such as hydrogen peroxide (H_2O_2) (Giné-Bordonaba et al., 2019; Huan et al., 2016; Jimenez et al., 2002). Generally, ROS are considered as normal by-products of the plant aerobic metabolism and are produced in different organelles within the cell (i.e. mitochondria (Huang et al., 2016)). ROS are, by definition, reactive molecules capable of oxidising and modifying some cellular components altering their normal functioning (Apel and Hirt, 2004). To counteract the negative effects of ROS accumulation, the plant has multiple ROS-scavenging mechanisms to ensure an adequate ROS homeostasis. Antioxidant molecules, such as ascorbic acid, glutathione, carotenoids, phenolic compounds and tocopherols, as well as enzymes, such as superoxide dismutase (SOD), peroxidase (POX)

ascorbate peroxidase (APX), catalase (CAT), and glutathione peroxidase (GPX), play an essential role in ROS scavenging mechanisms in plants and fruits (Apel and Hirt, 2004).

Besides their negative effects in plant cells, specific ROS, such as $^1O_2$, H_2O_2, $O_2^{\cdot-}$ and $^{\bullet}OH$, are deemed to be also key signaling molecules orchestrating multiple biological processes within the fruit including fruit development as well as the plant/fruit response to both biotic and abiotic stresses (Fichman and Mittler, 2020). In fact, ROS have been described to switch on the ethylene biosynthesis through the activation of MPK6, leading to the activation of ethylene response factors (ERFs) (i.e. ERF1 and ERF6), which in turn activate ROS-related gene expression easing the plant to counteract both biotic and abiotic stresses (Müller and Munné-Bosch, 2015). Also, evidence suggests an interaction between ROS and not only ethylene but other hormones regulating basic aspects of plant development. For instance, sunflower seed germination is regulated by the interaction of ROS with ethylene and abscisic acid (ABA) (El-Maarouf-Bouteau et al., 2015). Proof of such interactions during fruit development are however less abundant. In raspberries, application of ABA after fruit set modulates the ascorbate/dehydroascorbate (AsA/DHA) ratio in young berries and more than doubles AsA pools in ripe fruit by altering ascorbate oxidation and recycling through the activities of specific AsA-related antioxidant enzymes (Miret and Munné-Bosch, 2016).

In peach, Huan et al., (2016) described the potential role of ROS in regulating peach fruit development and ripening as well as the involvement of antioxidant genes and enzymes. However, only specific enzymes/genes (SOD, GPX and CAT) were considered in the above-mentioned study making it difficult to comprehensively evaluate the involvement of ROS and ROS-scavenging systems in nectarine fruit development. In other fruit, antioxidant enzymes are also though to play an important role yet showing species-specific changes along fruit development/ripening (López-Huertas and Palma, 2020; Singh et al., 2021).

To date, no comprehensive studies exist regarding changes in ROS-scavenging systems and their possible regulation during nectarine fruit development and ripening. Accordingly, the aim of this study was to investigate changes of both enzymatic and non-enzymatic ROS scavengers during 'Diamond Ray' nectarine development and ripening both at the enzymatic, metabolic and gene expression level.

2. Material and Methods

2.1. Plant material and experimental design

Experiments were conducted with 'Diamond Ray' nectarines (*Prunus persica* (L.) Batch) obtained from a commercial orchard located in Gimenells (Lleida, Catalonia, NE Spain). Fruit free of physical injuries and rot were picked at successive developmental stages (S1 = 39, S2 = 70, S3 = 94 and S4 = 121 days after full bloom (DAFB)), being full bloom the stage when at least 50% of flowers were open. After each harvest, nectarines were immediately transported to IRTA facilities under controlled conditions (20 °C). Upon arrival at the laboratory, fruit were separated into two different batches of 20 fruit each depending on whether they were used for: i) morphological and physiological (ethylene production and respiration rate) analysis, ii) biochemical and gene expression analysis. For the later, samples of pulp tissue from 4 individual replicates of 5 fruit each, were frozen in liquid nitrogen and kept at -80 ºC until further biochemical and molecular analysis.

2.2. Determination of fruit development, ethylene production and respiration rate

Twenty fruit were used for weight measurements by using a digital balance and expressed in grams (g), whereas fruit diameter was determined at the equatorial section of the fruit with an electronic digital calliper (Powerfix, Ilford, UK) and expressed in millimetres (mm). Additional samplings for fruit weight and diameter were done at regular intervals from 0 to 121 DAFB. Ethylene production and fruit respiration were determined as described

elsewhere (Baró-Montel et al., 2021). Four replicates of 5 fruit each, per sampling, were placed in sealed flasks of different volumes (depending on the developmental stage), in an acclimatised chamber at 20 °C, equipped with a silicon septum for sampling the gas of the headspace after 2 h incubation.

2.3. Determination of H_2O_2 and antioxidant activity

Hydrogen peroxide levels were determined as described by Giné-Bordonaba et al. (2017) using the PeroxiDetect Kit (Sigma Aldrich, USA) colorimetric assay and following the manufacturer's instructions. The content was expressed as μmol g^{-1} of fresh weight.

Antioxidant capacity of the fruit was determined using frozen tissue by the Ferric Reducing Antioxidant Power (FRAP) assay as described in recent works (Giné-Bordonaba et al., 2016) and the results expressed as mg Fe^{2+} g^{-1} FW.

2.4. Measurement of ROS-scavenging enzymes activity

Peroxidase (POX, EC 1.11.1.7) was extracted mixing 5 g of frozen pulp with 10 mL of phosphate buffer (100 mM, pH 6) with 0.5 mM cysteine and 0.5 g of PVPP and centrifuged at 20,000 x *g* for 15 min at 4 °C. A 2.5 mL of supernatant was loaded into a Sephadex G-25 column (PD 10; Pharmacia, Madrid, Spain) that had previously been equilibrated with 10 mL phosphate buffer (100 mM, pH 6) and the enzyme was eluted with 3.5 mL of the same buffer. POX activity was determined as described by Giné-Bordonaba et al. (2017).

Ascorbate peroxidase (APX; EC 1.11.1.11) extraction, 5 g of frozen pulp was mixed with 15 mL of 100 mM base phosphate buffer (pH 7.5) containing 0.8 mM ascorbic acid and 1 mM EDTA. The mixture was centrifuged at 10,000 x *g* for 15 min at 4 ºC (Collazo et al., 2018). APX activity was determined at 290 nm during 10 min by monitoring the H_2O_2-dependent decomposition of ascorbate in a mixture containing 20 μL of supernatant and

280 µL of a reaction solution containing 0.22 mM ascorbic acid, 1 mM EDTA and 1 mM H_2O_2 (Nakano and Asada, 1981).

For the extraction of superoxide dismutase (SOD, EC 1.15.1.1) and catalase (CAT, EC 1.11.1.6), 5 g of flesh tissue were homogenized in 15 mL 0.1 M potassium phosphate buffer (pH 7.8), 2 mM DTT, 5% (w/v) PVPP, 0.1 mM EDTA and 1.25 mM polyethylene glycol (Giné-Bordonaba et al., 2017). The homogenate was centrifuged at 20,000 x *g* for 15 min at 4 ºC and then a 2.5 mL aliquot was loaded into a Sephadex G-25 column (PD 10; Pharmacia, Madrid, Spain) equilibrated with 10 mL 0.1 M phosphate buffer (pH 7.8). The enzymes were eluted with 3.5 mL of the same buffer. The resulting supernatant was used as an enzyme extract to determine enzyme activity. SOD activity was assayed by measuring its ability to inhibit the photochemical reduction of nitrobluetetrazolium (NBT) as described elsewhere (Giné-Bordonaba et al., 2017). One unit of SOD (Unit of activity; UA) was considered the amount of enzyme required to inhibit NBT reduction by 50%. CAT activity was measured by the Claiborne (1985) method following the disappearance of H_2O_2 at 240 nm. Except for SOD (see above), enzyme activity was expressed in activity Units (U) per milligram of protein, with one U representing the quantity of enzyme responsible for a change in 1 absorbance unit per minute.

2.5. Extraction and quantification of ascorbic acid

Ascorbic acid (AsA) and total ascorbic acid (AsA + DHA) were extracted and analysed as described by Fernández-Cancelo et al., (2021). Dehydroascorbic acid (DHA) content was calculated by difference between total ascorbic acid and ascorbic acid.

2.6. Extraction and quantification of carotenoids and chlorophylls

Carotenoids and chlorophylls were extracted based on the method described by Alagoz et al. (2020) by mixing 125 mg of freeze-dried flesh tissue with 800 µL of acetone-ethyl

167 acetate (6:4, v/v) solution containing 0.1% butylated hydroxytoluene (BHT), and 0.1%
168 canthaxanthin (0.5 mg mL^{-1}) as internal standard. An equal volume of water was added,
169 samples were mixed by inversion, and centrifuged 5 min at 12,000 x *g* at 4 ºC. The upper
170 phase was collected and centrifuged again 5 min at 12,000 x *g* at 4 ºC. The organic extract
171 was filtered through a 0.22 μm filter and injected (20 μL) on an Agilent 1260 Infinity II
172 liquid chromatograph UHPLC fitted with a YMC C30 Carotenoid column (250 mm × 4.
173 mm i.d., 3 μm; Teknokroma, Barcelona, Spain) and a guard column of the same material
174 (10 mm × 4.0 mm, 3 μm). Separation was carried out at a flow rate of 1 mL/min using a
175 binary-gradient elution initially composed by 95% methanol and 5% methyl tert-butyl
176 ether (MTBE), which was increased linearly to 25% MTBE in 12 min, then raised to 65%
177 in 23 min, and finally elevated to 100% in 10 min and maintained for 10 min. The
178 temperature of the column was kept at 25 °C and the sample compartment was
179 refrigerated at 10 °C. Detection was performed at 454 nm yet the online spectra was
180 acquired in the 330-700 nm wavelength range with a resolution of 1 nm. Carotenoids and
181 chlorophylls were identified according to their retention time, spectral features, and ratios
182 of maximum absorption peaks (λ). Identified compounds were quantified using a
183 calibration curve prepared with a canthaxanthin standard stock solution and their
184 concentration were expressed as μg Canthaxanthin Equivalents (CXE) g^{-1} FW.

185 **2.7. Quantification of specific phenolic compounds**

186 Individual phenolic compounds from pulp tissue were quantified from the same extracts
187 used for antioxidant capacity determination. The methanolic extract was filtered through
188 a 0.22 μm filter and injected (5 μL) on an Agilent 1260 Infinity II liquid chromatograph
189 UHPLC fitted with a Waters XSelect HSS T3 (4.6x100 mm, 2.5 μm; Waters, Barcelona,
190 Spain) and a guard column Waters XSelect HSS T3 VanGuard (3.9x5 μm, 3.5 μm).

Separation was carried out at a flow rate of 0.75 mL/min using a mobile phase consisting in 0.1% acetic acid in water (A) and 0.1% acetic acid in acetonitrile (B). The gradient program was held for the first 2 min at 6% B, increased linearly to 12% B in 3 min, then raised to 30% B in 29 min, and finally elevated to 100% B in 6 min and maintained at 100% B for 5 min. The temperature of the column was kept at 40 °C and the sample compartment was refrigerated at 10 °C. Detection was performed at 280, 320 and 520 nm yet the online spectra was acquired in the 220-650 nm wavelength range with a resolution of 0.5 nm. Phenolic compounds were identified according to their retention time, spectral features, and ratios of maximum absorption peaks (λ) (Tomás-Barberán et al., 2001; Ribas-Agustí et al., 2011). The identification of phenolic compounds was confirmed by Mass Spectrometry (MS). Parent molecular ions were obtained by using MS scan mode whereas MS^2 daughters mode was used to obtain their fragmentation patterns, with argon as collision gas and 20-30V as collision energies. Quantification was performed using calibration curves prepared with standard stock solutions of cyanidin-3-O-glucoside, chlorogenic acid, catechin, quercetin-3-O-glucoside and their concentration were expressed as mg g^{-1} FW. Detected phenolic acids and quercetin-derivatives were quantified using chlorogenic acid and quercetin-3-O-glucoside standard curves.

2.8. RNA extraction and qPCR analysis

RNA was extracted using the Spectrum™ Plant Total RNA Kit (Sigma-Aldrich, St Louis, MO, USA) following the manufacturer's recommendation. Both the RNA integrity and the absence of contaminant DNA were determined by electrophoresis on an agarose gel by staining with GelRed™ Nucleic Acid Gel Stain (Biotium, Hayward, CA, USA). The cDNA synthesis was performed on 1 µg of RNA using the SuperScript IV First-Strand Synthesis System (Invitrogen, Carlsbad, CA, USA). The reaction mix consisted of the KAPA SYBR® Fast qPCR Master Mix (Kapa Biosystems, Inc., Wilmington, USA), 100 nM of each primer

and the corresponding diluted cDNA. The reaction was performed on a 7500 Real Time PCR System (Applied Biosystems) with the following conditions: 10 s at 95 ºC followed by 40 cycles of 95 ºC during 15 s and 60 ºC during 1 min. A non-template control (NTC) was included by using DNA-free water instead of cDNA. A melt curve analysis was performed to check primer specificity by including a final amplification cycle at 95 °C for 15 s, 60 °C for 1 min, 95 °C for 30 s and 60 °C for 15 s. Primers used in this study were retrieved from the literature or designed *de novo* when indicated (Supplementary Table S1). The *translation elongation factor* 2 (*TEF2*) was used for nectarine samples due to its high statistical reliability (Tong et al., 2009). Relative gene expression was expressed as Mean Normalised Expression (MNE) according to Muller et al. (2002).

2.9. Data analysis

Data were subjected to analysis of variance (ANOVA) using JMP® (v. 13.1, SAS Institute Inc., Cary, NC). Means were compared by analysis of variance (ANOVA). When the analysis was statistically significant, the Tukey's HSD test at the level $p \leq 0.05$ was performed for comparison of means along fruit development/ripening for gene expression, enzymatic activities, and metabolites. Correlations were made only with variables that shown significant differences between developmental stages using the Pearson's product moment correlation ($p \leq 0.05$) by using the 'corrplot' package (Taiyun and Simko, 2021) within R 3.4.0 software. Hierarchical cluster analysis (HCA), based on Ward's method (with 95% confidence) between different developmental stages was also used to construct the similarity dendrograms and heat-maps.

3. Results

3.1 Ethylene production, respiration and ROS-mediated signaling during fruit development and ripening

The diameter of 'Diamond Ray' nectarine fruit was monitored from 0 to fully ripe fruit (121 DAFB; Fig. 1) showing a double-sigmoid growth curve. The first growth phase lasted approximately 58 days with an average growth rate of 0.56 mm per d ($R^2 = 0.95$) until fruit reached a diameter of 32.5 mm. A second growth phase, coinciding with the pit hardening, registered an average growth rate of 0.29 mm per d, until fruit reached 34.8 mm. Finally, the third phase, the period of cell enlargement, displayed a rapid fruit growth rate with values of 0.67 mm per d ($R^2 = 0.98$), being 1.2-fold greater than the growth rate observed in the first growth phase. To further understand the biochemical changes accompanying the described fruit growth and ripening stages, four different sampling points corresponding to clearly different phenological phases (S1-S4; Fig. 1A) were investigated in this study. Both ethylene production and respiration rate were lower in periods of arrested or reduced fruit growth as in S2 in comparison to the data observed during periods of fast fruit growth (S1, S3 and S4). Indeed, the highest ethylene production and respiration rates were observed at S1 (0.27 µL C_2H_4 Kg^{-1} h^{-1} and 0.31 mg CO_2 Kg^{-1} h^{-1}, respectively).

Gene expression analysis of the ethylene and ROS-dependent transcription factors *PpERF1a* and *PpERF1b* (Fig. 1D and 1E), showed higher expression levels at earlier developmental stages (S1 and S2 for *PpERF1a* and S2 for *PpERF1b*). In detail, expression levels of *PpERF1*a were similar at S1 and S2, and 1.9 and 1.6-fold higher if compared to S3 and S4 stages, respectively. Regarding *PpERF1b*, expression levels increased by 1.5-fold from S1 to S2 to significantly decrease thereafter by 1.9 and 2.4-fold at S3 and S4, respectively.

3.2 Changes in ROS-scavenging compounds/enzymes and gene expression during fruit development and ripening

H_2O_2 levels linearly increased as the fruit developed and ripened on-tree with values at S4 being 5.2-fold greater than at S1. In contrast to the huge differences encountered for H_2O_2, the activity of SOD remained relatively unchanged throughout fruit development/ripening. A similar pattern was observed for CAT, responsible to catalyse the decomposition of H_2O_2 to water and oxygen. In contrast, POX activity remained relatively high from S1 to S3 (181.84-230.61 U mg^{-1} protein) and significantly dropped later at the S4 stage (39.77 U mg^{-1} protein). The activity of APX, was nearly 3-fold greater at S1 than at the other fruit developmental stages. Changes in APX, were in line with the observed levels of AsA and DHA being the lowest (0.0009 mg g^{-1}) and greatest (0.1340 mg g^{-1}), respectively, at S1.

The expression of genes involved in ascorbate metabolism or the antioxidant enzymes detailed above was generally poorly correlated with the equivalent metabolite concentration or enzymes activity (Supplementary Fig. 5). Significant differences were found for the expression of all genes along the different fruit developmental stages except for *PpDHAR* and *PpSODb* that showed no changing pattern along fruit development (Fig. 2 and Supplementary Fig. 1). The highest gene expression levels were observed for *PpCAT*, and especially at S2 (29.13 MNE) and S3 (30.27 MNE). For SOD, three different paralogs were considered based on their diverse cellular localization among ROS producing cellular compartments/organelles (Supplementary Table 1). Significant differences were found between paralogs at each fruit developmental stage. The chloroplastic *PpSODa* showed the greatest expression levels at S1 progressively declining thereafter. As said, the mitochondrial *PpSODb*, did not show a differential expression pattern while *PpSODc*, located in the cytoplasm, showed the greatest gene

expression level at S2 and S3 (in average 0.14 MNE). Two different paralogs were also considered for APX (*PpAPXa*-cytoplasmatic and *PpAPXb*-chloroplastic). *PpAPXa* gene expression levels changed in parallel to the levels of H_2O_2, whereas *PpAPXb* gene expression levels were low at S1 and increase thereafter to remain at relative constant levels from S2 to S4. *PpMDHAR* gene expression levels peak at S2 to decline in more advanced fruit developmental stages. Finally, the expression levels of *PpPOX* were in line to its counterpart enzyme showing its highest levels at S1 and S2, and the lowest gene expression levels at S3.

3.3 Changes in carotenoids and related-gene expression during fruit development and ripening

β-carotene and violaxanthin were the predominant carotenoids at early fruit developmental stages (S1; 0.28 and 0.22 μg g^{-1} FW, respectively), the concentration of which gradually decreased as the fruit developed/ripened (Fig. 3). At S4, the content of both lutein and violaxanthin was negligible (lutein (0.009 μg g^{-1} FW) and violaxanthin (0.007 μg g^{-1} FW)). Other carotenoids such as neoxanthin followed a similar trend and were degraded as the fruit developed and ripened. In contrast, β-cryptoxanthin and zeaxanthin tended to accumulate as the fruit developed and ripened (5.66 and 5.56-fold higher values, respectively, at S4 than at S1) being the majoritarian carotenoids at the fully ripe stage (S4).

The expression of five genes involved in different steps within the carotenoid biosynthetic pathway were analysed by RT-qPCR (Supplementary Table 1). *PpB-CHX* and *PpE-CHX*, the genes encoding for the enzymes responsible to convert α-carotene and β-carotene to Lutein and β-cryptoxanthin, respectively, showed clear differences in their expression level during fruit development/ripening (Fig. 3 and Supplementary Fig. 2). For instance,

no significant differences were found for the expression levels of *PpE-CHX* whereas a constant increase in the expression of *PpB-CHX* was observed paralleling the fruit development/ripening. For all the other analysed genes (*PpVDE*, *PpZEP* and *PpNCED*) the expression levels were greatest at later fruit developmental stages and specially at S4.

3.4 Changes in specific phenolic compounds and related-gene expression during fruit development and ripening

Up to nine different phenolic compounds were detected yet depending on the fruit developmental stage (Supplementary Table 2). For most compounds, the highest concentration was detected at S1 (Fig. 4), except for the anthocyanin cyanidin-3-O-glucoside which remains constant during fruit development. Quercetin-derivatives and p-coumaroylquinic acid isomers were present in the first three developmental stages studied herein, while absent at S4. On the other hand, at S4, the main phenolic compounds detected were chlorogenic acid (0.079 mg g^{-1} FW), neochlorogenic acid (0.043 mg g^{-1} FW), cyanidin-3-O-glucoside (0.014 mg g^{-1} FW) and catechin (0.002 mg g^{-1} FW).

The expression of eight genes involved in the biosynthesis of several phenylpropanoids (Supplementary Table 1) was investigated along fruit development/ripening. Our results showed that for all targeted genes, except for *PpCOMT*, the highest and lowest gene expression was observed at S2 and S4, respectively (Fig. 4 and Supplementary Fig. 3). In detail, expression levels of *PpPAL* were, in average, 98.2-fold higher at S2 if compared to other developmental stages analysed herein. Genes located downstream the phenylpropanoid biosynthetic pathway and responsible, for example, for the biosynthesis of dihydroflavonols, flavonols and anthocyanins (*PpF3'H*, *PpFLS* and *PpANS*), were also highly expressed at S2.

3.5 Overall ROS-scavenging transcriptomic and biochemical changes associated to fruit development and ripening

To further investigated the changes in the expression of genes (Fig. 5A) and metabolites (Fig. 5B) related to antioxidant metabolism, a hierarchical cluster analysis was performed integrating separately all the gene expression (n= 384; 24 genes x 4 developmental stages per replicate) and metabolite (n=448; 28 metabolites x 4 developmental stages per replicate) data. A clear separation of the different fruit developmental stages was observed based on the targeted gene-expression levels (Fig. 5A). S1, S3 and S4 samples were clearly separated from S2 (Fig. 5A) suggesting the most pronounced transcriptomic changes occurred at S2 (70 DAFB). Two-way clustering analysis revealed 4 different gene clusters responsible for the differentiation of the samples based on the fruit developmental stage. Cluster 1 included 5 genes related with the biosynthesis of phenylpropanoids and *PpERF1b* (Fig. 5A) which were highly expressed almost exclusively at S2. Cluster 2 included 5 genes belonging to different metabolic pathways (carotenoids biosynthesis, antioxidant enzymes and *PpERF1a*) being highly expressed both at S1 and S2. Cluster 3 included genes involved downstream the phenylpropanoid or carotenoid biosynthetic pathways as well as CAT and a SOD paralog together with genes involved in ascorbate metabolism. The expression of genes within this cluster was highest at S2 and S3. Finally, cluster 4 included a set of genes (3 genes involved in the metabolism of carotenoids (Fig. 5A) as well as an APX paralog and *PpCOMT*, highly expressed only in ripe fruit (S4).

A different separation of the fruit developmental stages than that detailed above was observed when considering metabolite contents (Fig. 5B). Indeed, poor correlations were observed between gene expression levels and metabolite contents (Supplementary Fig. 5). Most metabolites were present at higher concentrations at either S1 (75% of the

363 measured phenylpropanoids and 4 out of the 6 identified carotenoids) or S4 (ethylene,
364 ascorbate, H_2O_2, etc). Three main metabolite clusters were responsible for the separation
365 of the samples without any clear association regarding the different targeted metabolic
366 pathways.

4. Discussion

4.1 Ethylene and respiration may contribute to an early generation of ROS during 'Diamond Ray' development

Nectarine fruit is a rich source of antioxidants (Redondo et al., 2017) including ascorbate, carotenoids, and phenolics. While all these compounds are beneficial for human health, antioxidants, including both enzymatic and non-enzymatic, are also required within the cell to enable a correct balance between ROS and antioxidant levels (redox homeostasis). ROS are generated during normal metabolic processes, such as fruit development and ripening, acting as both signaling molecules responsible of tuning cellular biological functions (i.e. promoting cellular proliferation and differentiation) but also as toxic by-products generated during aerobic metabolism (Mittler, 2017). Although fruit are characterized by their reduced photosynthetic activity (Blanke and Lenz, 1989), the climacteric nature of some fruit species involves an increased respiration rate that ultimately leads to an enhanced ROS production (Kan et al., 2010), being mainly $^{1}O_2$ and $O_2^{\cdot-}$. In fact, in plants tissues, the main sources of ROS are the chloroplastic photosynthesis, the mitochondrial respiration and the peroxisomal photorespiration cycle (Decros et al., 2019). Such generated ROS are involved in many signaling processes, modulating the cell transcriptome to finally enable a correct fruit development and ripening (Muñoz and Munné-Bosch, 2018) but also to ensure a correct response to many abiotic and biotic stresses (Apel and Hirt, 2004).

In this sense, while numerous studies are available quantifying specific antioxidants during peach/nectarine development and ripening (Andreotti et al., 2008; Cao et al., 2017; Huan et al., 2016), scarce comprehensive information exists on how ROS-scavenging enzymes and compounds change during fruit development and ripening.

Nectarines are considered climacteric fruit, which implies and absolute dependence of the phytohormone ethylene to ripen. The analysis of ethylene and respiration dynamics during the development of 'Diamond Ray' nectarines revealed that ethylene production, and to a lower extent the respiration rate, was greatest in the period of maximum fruit growth (Fig. 1), a phenomenon that seems to be conserved among different cultivars (Baró-Montel et al., 2021) and to some extent among Rosaceae spp. i.e. apples (Giné-Bordonaba et al., 2019). Our data suggest a parallelism between the fruit ethylene production and the respiration rate as previously described for other cultivars (Ferrer et al., 2005), the later process being a well-known source of ROS. A wide range of ROS, including $O_2^{\cdot-}$ generated via aerobic metabolism, can mediate the regulation of ROS-responsive genes either by promoting the ethylene biosynthetic pathway which in turn activates ERFs (i.e. ERF1 and ERF6) or by directly activating such transcription factors (Müller and Munné-Bosch, 2015). Among all ERFs genes already characterized in peach during fruit ripening (Wang et al., 2017), we selected *PpERF1* given that this gene showed the highest homology with Arabidopsis *AtERF1* and *AtERF6* genes. In fact, the increased respiration rate occurring during the early developmental stages (S1) of 'Diamond Ray' nectarines likely resulted in the upregulation of both *PpERF1a* (at both S1 and S2 stages) and *PpERF1b* (at S2) (Fig. 1). $O_2^{\cdot-}$ within the cells can be dismutated to H_2O_2 by the action of SODs (Decros et al., 2019). In our study, dismutation of $O_2^{\cdot-}$ to H_2O_2 (SOD activity) was somehow constant throughout fruit development and ripening, yet higher levels of H_2O_2 were observed as the fruit developed/ripened (Fig. 2). In fact, the significant increase of H_2O_2 levels at S4 stage is in line with the fact that ROS content picks at the onset of fruit ripening (Muñoz and Munné-Bosch, 2018) and to the observed increase of these compounds concomitant to an enhanced ACC oxidase and polygalacturonase transcripts in an aim to favour fruit softening (Jimenez et al., 2002).

4.2 A decrease in POX is paralleled by the accumulation of H_2O_2 likely triggering fruit ripening.

Our data also suggest that specific ROS, including H_2O_2, may be more efficiently scavenged by the fruit at earlier developmental stages not by the action of SOD but through other scavenging mechanisms. Huan et al. (2016) reported an increased SOD activity in peaches at 70 DAFB proceeded by a further decrease paralleling fruit development and ripening. A peak in SOD activity has been earlier reported at the colour turning stage for olives (López-Huertas et al., 2021) or white stage in strawberry (López et al., 2010) while no drastic changes were reported during tomato ripening (Jimenez et al., 2002). Such conflicting information existing for most antioxidant enzymes along fruit ripening (Jimenez et al., 2002; López-Huertas et al., 2021) strongly suggest a species-specific or even a cultivar-specific regulation occurring already at the transcript level (Fig. 2). The lack of correlation between SOD activity and H_2O_2 accumulation detailed herein also suggest that H_2O_2 may arise from other sources different that SOD such as pH-dependent dismutation or directly produced by the photosynthetic electron transport chain components (Khorobrykh et al., 2015).

Higher plants contain antioxidant enzymes encoded by families of homologous genes, which present unique properties in terms of their expression and subcellular localization. Different *PpSOD* paralogs with diverse cell localization (Supplementary Table 1) were analysed in this study. While the mitochondrial *PpSODb* paralog did not significantly change along the fruit development, both *PpSODa* and *PpSODc* (chloroplastic and cytosolic localization, respectively) tended to decrease during fruit development and ripening. The different transcript behaviours could in part explain why SOD activity (Fig. 2) finally remained invariable. Indeed, it is already demonstrated that many other reasons, including the protein turnover and the different regulation at transcriptional or

translational level could explain such an absence of correlation between mRNA levels and protein amount/activity (Greenbaum et al., 2003).

Regarding the POX activity, our results show a significant decrease during the ripening phase (S3-S4; Fig. 2) in line with that described for tomato and strawberry (López et al., 2010; Mondal et al., 2004). However, in mango, apple and banana fruit, such antioxidant enzyme activity increases as the fruit ripen (reviewed in Decros et al. (2019)). Higher levels of POX during the pit hardening period (S1-S2) have previously been described in the literature (Abeles and Biles, 1991). In our study, the decline in POX activity paralleled the accumulation of H_2O_2 explaining to some extent the observed accumulation of this compound as the fruit developed/ripened. On the other hand, *PpCAT* did not present a clear trend and remained constant as the fruit develops, although transcript levels for this specific gene peaked at both S2 and S3 stage.

In line with H_2O_2, the levels of ascorbic acid were also higher at later developmental stages than at S1 stage (Fig. 2). These results could be in part explained by the reduced APX activity at S2-S4 stages if compared to S1 (Fig. 2). Again, the transcript levels of both paralogs of *PpAPX* analysed herein (the cytoplasmic *PpAPXa* and the chloroplastic *PpAPXb*) did not correlated with the activity of the enzymes, pointing out that other paralogs may be responsible of the final APX protein/activity or that the regulation of APX occurs at the translational but not at the transcriptional level. Such lower APX activity along the fruit development resulted in a decreased conversion of ascorbate to its reduced forms, monodehydroascorbic acid (MDHA) and DHA (Fig. 2) as well as in an increased *PpMDHAR* transcript levels that could in turn explain the increased AsA/DHA redox ratio. Early fruit developmental stages presented a low AsA/DHA ratio while as the fruit developed and ripened, AsA levels increased and the fruit shifted towards a lower AsA/DHA ratio as previously described for grape berries (Melino et al., 2009).

ROS, not only by themselves but through their crosstalk with several phytohormones, may orchestrate fruit development and ripening (reviewed in Devireddy et al. (2021)). As mentioned above, the fruit H_2O_2 pool increased concomitantly with the visual skin colour changes (Fig. 1), supporting the putative role of this molecule on the regulation of the chloroplast to the chromoplast transition being the later transition involved in the regulation of fruit ripening (Ling et al., 2021).

4.3 Most carotenoids and phenylpropanoids drastically decreased during fruit development and ripening

In addition to the enzyme-mediated scavenging mechanisms described above, the harmful action of ROS can be mitigated by the action of antioxidant molecules such as carotenoids and phenylpropanoids. Carotenoids are synthesised and stored in the chloroplast where they act as accessory light-harvesting pigments dissipating energy excess, as well as, neutralizing singlet oxygen species produced during photosynthesis (Havaux, 2014). Traditionally and based on available data on tomatoes, it has been considered that during fruit ripening, chlorophyll is progressively degraded while carotenoid synthesis is favoured (Llorente et al., 2016). However, total carotenoids decreases concomitantly with chlorophyll levels during fruit development in other Rosaceae species (Ma et al., 2014). Analysis of the flesh pigment content of the nectarine 'Diamond Ray' showed a linear decrease of chlorophylls during fruit development (Supplementary Fig. 4), while the total carotenoid content (sum of the individual carotenoids detected; Fig. 3) decreases by one third between S1 and S2 and remained constant thereafter. The analysis of specific carotenoid compounds during the development of 'Diamond Ray' nectarines revealed that while those pigments typical of leaves and small fruits such as lutein, β-carotene, neoxanthin and violaxanthin tend to decrease as 'Diamond Ray' nectarines developed and ripened, β-cryptoxanthin and zeaxanthin levels increased progressively (Fig. 3), in line with previous studies

demonstrating its accumulation in ripe fruit (Rodrigo et al., 2013). Such results together with the available literature regarding carotenoid changes during peach/nectarine development and ripening strongly suggests that carotenoid metabolism is cultivar dependent. Opposed to that observed for antioxidant enzymes, the carotenoid content was in line with the transcript levels of the genes involved in their biosynthesis/degradation (Fig. 3). Thus, the reduced levels of β-carotene and neoxanthin as the fruit developed could be directly explained by the increased expression of *PpB-CHX* and *PpNCED* at S4 (Fig. 5A), respectively. Based on the observed upregulation of *PpNCED*, it is likely to speculate that ABA may increase as the fruit developed and ripened in a similar way to that reported for other stone fruit (Tijero et al., 2019). Moreover, the increased levels of *PpVDE* could be in part responsible of the increased content of zeaxanthin regardless the induction of *PpZEP* along fruit development. On the other hand, given that the expression of the *PpE-CHX* gene did not vary during development, it is feasible to hypothesize that the decrease in lutein levels may be caused by the activation of carotenoid catabolic pathways mediated by carotenoid cleavage dioxygenases (Ma et al., 2014).

Besides carotenoids, phenylpropanoid compounds are widely known for their antioxidant capacity. From all the compounds identified, catechin, quercetin-derivatives and chlorogenic/neochlorogenic were clearly accumulated during the first developmental stages, while all of them tend to decrease thereafter as the fruit developed/ripened. Such profile is in line with previous studies and also with other species such as apricots (Dragovic-Uzelac et al., 2007). On the other hand, anthocyanins concentration remained unchanged during the fruit developmental stages. At the S2 stage there was an evident upregulation of all the genes involved in the biosynthesis of these compounds, which lead us to hypothesise that phenylpropanoid changes along fruit development and ripening are regulated via a possible positive feed-back mechanism.

5. Conclusions

To the best of our knowledge this is the first study providing comprehensive information regarding a wide range of ROS-scavenging systems along nectarine fruit development and ripening. Overall, our results demonstrate that nectarines (cv. 'Diamond Ray') exhibited, at earlier developmental stages (S1; 39 DAFB), an increase in the respiration rate likely accompanied by an oxidative burst. This burst may act as a signaling cascade by activating both the ethylene biosynthetic and signaling pathways that may ultimately activate different ROS-responsive genes (Fig. 6) or the biosynthesis of specific antioxidant compounds. However, as the fruit develops, the respiration rate decreases and hence the amount of ROS generated, other than H_2O_2, likely decreased, leading to a reduction of ERF1 and hence potentially accounting for the lower levels of antioxidants (Fig. 6). Such decrease in enzymatic and non-enzymatic antioxidants results in the inability of the fruit to scavenge H_2O_2, which accumulates during nectarine development.

Acknowledgements

This work was partly supported by the CERCA programme from the Generalitat de Catalunya. We are grateful to Dolors Ubach and Elisabeth Duaigües for their technical assistance. Thanks are also given to the Ministerio de Ciencia e Innovación and European Regional Development Fund (ERDF) for the predoctoral fellowship awarded to PFC (BES-2017-080741).

Conflict of interests

All authors declare no conflict of interest.

Author contributions

JGB and RT conceived and designed the experiment. NV, PFC and INL carried out the experimental procedures. CL, NT and GE assisted with the statistical analysis and data interpretation. NV, PFC and JGB drafted the manuscript and all other authors contributed in improving the final version of the manuscript.

References

Abeles, F.B., Biles, C.L., 1991. Characterization of peroxidases in lignifying peach fruit endocarp. Plant Physiol. 95, 269–273. https://doi.org/10.1104/pp.95.1.269

Alagoz, Y., Dhami, N., Mitchell, C., Cazzonelli, C.I., 2020. cis/trans Carotenoid extraction, purification, detection, quantification, and profiling in plant tissues, in: Plant and Food Carotenoids. Methods in Molecular Biology, Vol 2083. Humana, New York, NY. pp. 145–163. https://doi.org/10.1007/978-1-4939-9952-1_11

Andreotti, C., Ravaglia, D., Ragaini, A., Costa, G., 2008. Phenolic compounds in peach (*Prunus persica*) cultivars at harvest and during fruit maturation. Ann. Appl. Biol. 153, 11–23. https://doi.org/10.1111/j.1744-7348.2008.00234.x

Apel, K., Hirt, H., 2004. Reactive oxygen species: Metabolism, oxidative stress, and signal transduction. Annu. Rev. Plant Biol. 55, 373–399. https://doi.org/10.1146/annurev.arplant.55.031903.141701

Baró-Montel, N., Giné-Bordonaba, J., Torres, R., Vall-llaura, N., Teixidó, N., Usall, J., 2021. Scrutinising the relationship between major physiological and compositional changes during ‘Merrill O’Henry’ peach growth with brown rot susceptibility. Food Sci. Technol. Int. https://doi.org/10.1177/1082013220959988

563 Blanke, M.M., Lenz, F., 1989. Fruit photosynthesis. Plant, Cell Environ. 12, 31–46.
564 https://doi.org/10.1111/j.1365-3040.1989.tb01914.x

565 Brandi, F., Bar, E., Mourgues, F., Horváth, G., Turcsi, E., Giuliano, G., Liverani, A.,
566 Tartarini, S., Lewinsohn, E., Rosati, C., 2011. Study of "Redhaven" peach and its
567 white-fleshed mutant suggests a key role of CCD4 carotenoid dioxygenase in
568 carotenoid and norisoprenoid volatile metabolism. BMC Plant Biol. 11, 24.
569 https://doi.org/10.1186/1471-2229-11-24

570 Cao, S., Liang, M., Shi, L., Shao, J., Song, C., Bian, K., Chen, W., Yang, Z., 2017.
571 Accumulation of carotenoids and expression of carotenogenic genes in peach fruit.
572 Food Chem. 214, 137–146. https://doi.org/10.1016/j.foodchem.2016.07.085

573 Claiborne, A., 1985. Catalase Activity, in: CRC Handbook of Methods for Oxygen
574 Radical Research. CRC Press, pp. 283–284.

575 Collazo, C., Giné-Bordonaba, J., Aguiló-Aguayo, I., Povedano, I., Bademunt, A., Viñas,
576 I., 2018. *Pseudomonas graminis* strain CPA-7 differentially modulates the oxidative
577 response in fresh-cut 'Golden delicious' apple depending on the storage conditions.
578 Postharvest Biol. Technol. 138, 46–55.
579 https://doi.org/10.1016/j.postharvbio.2017.12.013

580 Dardick, C.D., Callahan, A.M., Chiozzotto, R., Schaffer, R.J., Piagnani, M.C., Scorza,
581 R., 2010. Stone formation in peach fruit exhibits spatial coordination of the lignin
582 and flavonoid pathways and similarity to *Arabidopsis* dehiscence. BMC Biol. 8, 1–
583 17. https://doi.org/10.1186/1741-7007-8-13

584 Decros, G., Baldet, P., Beauvoit, B., Stevens, R., Flandin, A., Colombié, S., Gibon, Y.,
585 Pétriacq, P., 2019. Get the balance right: ROS homeostasis and redox signalling in
586 fruit. Front. Plant Sci. 10. https://doi.org/10.3389/fpls.2019.01091

587 Devireddy, A.R., Zandalinas, S.I., Fichman, Y., Mittler, R., 2021. Integration of reactive
588 oxygen species and hormone signaling during abiotic stress. Plant J. 105, 459–476.
589 https://doi.org/10.1111/tpj.15010

590 Diretto, G., Frusciante, S., Fabbri, C., Schauer, N., Busta, L., Wang, Z., Matas, A.J., Fiore,
591 A., K.C. Rose, J., Fernie, A.R., Jetter, R., Mattei, B., Giovannoni, J., Giuliano, G.,
592 2020. Manipulation of β-carotene levels in tomato fruits results in increased ABA
593 content and extended shelf life. Plant Biotechnol. J. 18, 1185–1199.
594 https://doi.org/10.1111/pbi.13283

595 Dragovic-Uzelac, V., Levaj, B., Mrkic, V., Bursac, D., Boras, M., 2007. The content of
596 polyphenols and carotenoids in three apricot cultivars depending on stage of
597 maturity and geographical region. Food Chem. 102, 966–975.
598 https://doi.org/10.1016/j.foodchem.2006.04.001

599 El-Maarouf-Bouteau, H., Sajjad, Y., Bazin, J., Langlade, N., Cristescu, S.M., Balzergue,
600 S., Baudouin, E., Bailly, C., 2015. Reactive oxygen species, abscisic acid and
601 ethylene interact to regulate sunflower seed germination. Plant, Cell Environ. 38,
602 364–374. https://doi.org/10.1111/pce.12371

603 Fernández-Cancelo, P., Teixidó, N., Echeverría, G., Torres, R., Larrigaudière, C., Giné-
604 Bordonaba, J., 2021. Dissecting the influence of the orchard location and the
605 maturity at harvest on apple quality, physiology and susceptibility to major
606 postharvest pathogens. Sci. Hortic. (Amsterdam). 285, 110159.
607 https://doi.org/10.1016/j.scienta.2021.110159

608 Ferrer, A., Remón, S., Negueruela, A.I., Oria, R., 2005. Changes during the ripening of
609 the very late season Spanish peach cultivar Calanda: Feasibility of using CIELAB
610 coordinates as maturity indices. Sci. Hortic. (Amsterdam). 105, 435–446.

https://doi.org/10.1016/j.scienta.2005.02.002

Fichman, Y., Mittler, R., 2020. Rapid systemic signaling during abiotic and biotic stresses: is the ROS wave master of all trades? Plant J. 102, 887–896. https://doi.org/10.1111/TPJ.14685

Giné-Bordonaba, J., Cantín, C.M., Echeverría, G., Ubach, D., Larrigaudière, C., 2016. The effect of chilling injury-inducing storage conditions on quality and consumer acceptance of different *Prunus persica* cultivars. Postharvest Biol. Technol. 115, 38–47. https://doi.org/10.1016/j.postharvbio.2015.12.006

Giné-Bordonaba, J., Echeverria, G., Duaigües, E., Bobo, G., Larrigaudière, C., 2019. A comprehensive study on the main physiological and biochemical changes occurring during growth and on-tree ripening of two apple varieties with different postharvest behaviour. Plant Physiol. Biochem. 135, 601–610. https://doi.org/10.1016/j.plaphy.2018.10.035

Giné-Bordonaba, J., Echeverria, G., Ubach, D., Aguiló-Aguayo, I., López, M.L., Larrigaudière, C., 2017. Biochemical and physiological changes during fruit development and ripening of two sweet cherry varieties with different levels of cracking tolerance. Plant Physiol. Biochem. 111, 216–225. https://doi.org/10.1016/j.plaphy.2016.12.002

Greenbaum, D., Colangelo, C., Williams, K., Gerstein, M., 2003. Comparing protein abundance and mRNA expression levels on a genomic scale. Genome Biol. 4. https://doi.org/10.1186/gb-2003-4-9-117

Havaux, M., 2014. Carotenoid oxidation products as stress signals in plants. Plant J. 79, 597–606. https://doi.org/10.1111/tpj.12386

Hayama, H., Shimada, T., Fujii, H., Ito, A., Kashimura, Y., 2006. Ethylene-regulation of fruit softening and softening-related genes in peach. J. Exp. Bot. 57, 4071–4077.

Huan, C., Jiang, L., An, X., Yu, M., Xu, Y., Ma, R., Yu, Z., 2016. Potential role of reactive oxygen species and antioxidant genes in the regulation of peach fruit development and ripening. Plant Physiol. Biochem. 104, 294–303. https://doi.org/10.1016/j.plaphy.2016.05.013

Huang, S., Van Aken, O., Schwarzländer, M., Belt, K., Millar, A.H., 2016. The roles of mitochondrial reactive oxygen species in cellular signaling and stress response in plants. Plant Physiol. 171, 1551–1559. https://doi.org/10.1104/pp.16.00166

Jia, H., Jiu, S., Zhang, C., Wang, C., Tariq, P., Liu, Z., Wang, B., Cui, L., Fang, J., 2016. Abscisic acid and sucrose regulate tomato and strawberry fruit ripening through the abscisic acid-stress-ripening transcription factor. Plant Biotechnol. J. 14, 2045–2065. https://doi.org/10.1111/pbi.12563

Jiao, Y., Ma, R. juan, Shen, Z. jun, Yan, J., Yu, M. liang, 2014. Gene regulation of anthocyanin biosynthesis in two blood-flesh peach (*Prunus persica* (L.) Batsch) cultivars during fruit development. J. Zhejiang Univ. Sci. B 15, 809–819. https://doi.org/10.1631/jzus.B1400086

Jimenez, A., Creissen, G., Kular, B., Firmin, J., Robinson, S., Verhoeyen, M., Mullineaux, P., 2002. Changes in oxidative processes and components of the antioxidant system during tomato fruit ripening. Planta 214, 751–758. https://doi.org/10.1007/s004250100667

Kan, J., Wang, H. mei, Jin, C. hai, Xie, H. yan, 2010. Changes of reactive oxygen species and related enzymes in mitochondria respiratory metabolism during the ripening of peach fruit. Agric. Sci. China 9, 138–146. https://doi.org/10.1016/S1671-

2927(09)60077-8

Khorobrykh, S.A., Karonen, M., Tyystjärvi, E., 2015. Experimental evidence suggesting that H2O2 is produced within the thylakoid membrane in a reaction between plastoquinol and singlet oxygen. FEBS Lett. 589, 779–786. https://doi.org/10.1016/j.febslet.2015.02.011

Ling, Q., Sadali, N.M., Soufi, Z., Zhou, Y., Huang, B., Zeng, Y., Rodriguez-Concepcion, M., Jarvis, R.P., 2021. The chloroplast-associated protein degradation pathway controls chromoplast development and fruit ripening in tomato. Nat. Plants 7, 655–666. https://doi.org/10.1038/s41477-021-00916-y

Llorente, B., D'Andrea, L., Rodríguez-Concepción, M., 2016. Evolutionary recycling of light signaling components in fleshy fruits: new insights on the role of pigments to monitor ripening. Front. Plant Sci. 7. https://doi.org/10.3389/fpls.2016.00263

López-Huertas, E., Lozano-Sánchez, J., Segura-Carretero, A., 2021. Olive oil varieties and ripening stages containing the antioxidants hydroxytyrosol and derivatives in compliance with EFSA health claim. Food Chem. 342, 128291. https://doi.org/10.1016/j.foodchem.2020.128291

López-Huertas, E., Palma, J.M., 2020. Changes in glutathione, ascorbate, and antioxidant enzymes during olive fruit ripening. J. Agric. Food Chem. 68, 12221–12228. https://doi.org/10.1021/acs.jafc.0c04789

López, A.P., Gochicoa, M.T.N., Franco, A.R., 2010. Activities of antioxidant enzymes during strawberry fruit development and ripening. Biol. Plant. 54, 349–352. https://doi.org/10.1007/s10535-010-0061-8

Ma, J., Li, J., Zhao, J., Zhou, H., Ren, F., Wang, L., Gu, C., Liao, L., Han, Y., 2014.

Inactivation of a Gene Encoding Carotenoid Cleavage Dioxygenase (CCD4) Leads to Carotenoid-Based Yellow Coloration of Fruit Flesh and Leaf Midvein in Peach. Plant Mol. Biol. Report. 32, 246–257. https://doi.org/10.1007/s11105-013-0650-8

Melino, V.J., Soole, K.L., Ford, C.M., 2009. Ascorbate metabolism and the developmental demand for tartaric and oxalic acids in ripening grape berries. BMC Plant Biol. 9, 1–14. https://doi.org/10.1186/1471-2229-9-145

Miret, J.A., Munné-Bosch, S., 2016. Abscisic acid and pyrabactin improve Vitamin C contents in raspberries. Food Chem. 203, 216–223. https://doi.org/10.1016/j.foodchem.2016.02.046

Mittler, R., 2017. ROS Are Good. Trends Plant Sci. 22, 11–19. https://doi.org/10.1016/j.tplants.2016.08.002

Mondal, K., Sharma, N.S., Malhotra, S.P., Dhawan, K., Singh, R., 2004. Antioxidant systems in ripening tomato fruits. Biol. Plant. 48, 49–53. https://doi.org/10.1023/B:BIOP.0000024274.43874.5b

Müller, M., Munné-Bosch, S., 2015. Ethylene response factors: a key regulatory hub in hormone and stress signaling. Plant Physiol. 169, 32–41. https://doi.org/10.1104/pp.15.00677

Muller, P.Y., Miserez, A.R., Dobbie, Z., 2002. Short technical report processing of gene expression data generated. Gene Expr. 32, 1372–1379.

Muñoz, P., Munné-Bosch, S., 2018. Photo-oxidative stress during leaf, flower and fruit development. Plant Physiol. 176, 1004–1014. https://doi.org/10.1104/pp.17.01127

Nakano, Y., Asada, K., 1981. Hydrogen peroxide is scavenged by ascorbate-specific peroxidase in spinach chloroplasts. Plant Cell Physiol. 22, 867–880.

https://doi.org/10.1093/oxfordjournals.pcp.a076232

Palma, J.M., Corpas, F.J., Freschi, L., Valpuesta, V., 2019. Editorial: Fruit ripening: From present knowledge to future development. Front. Plant Sci. 10, 1–3. https://doi.org/10.3389/fpls.2019.00545

Ravaglia, D., Espley, R. V., Henry-Kirk, R.A., Andreotti, C., Ziosi, V., Hellens, R.P., Costa, G., Allan, A.C., 2013. Transcriptional regulation of flavonoid biosynthesis in nectarine (*Prunus persica*) by a set of R2R3 MYB transcription factors. BMC Plant Biol. 13. https://doi.org/10.1186/1471-2229-13-68

Redondo, D., Arias, E., Oria, R., Venturini, M.E., 2017. Thinned stone fruits are a source of polyphenols and antioxidant compounds. J. Sci. Food Agric. 97, 902–910. https://doi.org/10.1002/JSFA.7813

Reig, G., Iglesias, I., Gatius, F., Alegre, S., 2013. Antioxidant capacity, quality, and anthocyanin and nutrient contents of several peach cultivars [Prunus persica (L.) Batsch] grown in Spain. J. Agric. Food Chem. 61, 6344–6357. https://doi.org/10.1021/jf401183d

Ribas-Agustí, A., Gratacós-Cubarsí, M., Sárraga, C., García-Regueiro, J.-A., Castellari, M., 2011. Analysis of eleven phenolic compounds including novel p-coumaroyl Derivatives in lettuce (*Lactuca sativa* L.) by ultra-high-performance liquid chromatography with photodiode array and Mass Spectrometry Detection. Phytochem. Anal. 22, 555–563. https://doi.org/10.1002/pca.1318

Rodrigo, M.J., Alquézar, B., Alós, E., Medina, V., Carmona, L., Bruno, M., Al-Babili, S., Zacarías, L., 2013. A novel carotenoid cleavage activity involved in the biosynthesis of *Citrus* fruit-specific apocarotenoid pigments. J. Exp. Bot. 64, 4461. https://doi.org/10.1093/JXB/ERT260

Sherif, S., El-Sharkawy, I., Paliyath, G., Jayasankar, S., 2012. Differential expression of peach ERF transcriptional activators in response to signaling molecules and inoculation with *Xanthomonas campestris* pv. *pruni*. J. Plant Physiol. 169, 731–739. https://doi.org/10.1016/j.jplph.2012.02.003

Singh, V., Chahal, T.S., Grewal, S.K., Gill, P.S., 2021. Effect of fruit development stages on antioxidant properties and bioactive compounds in peel, pulp and juice of grapefruit varieties. J. Food Meas. Charact. 15, 2531–2539. https://doi.org/10.1007/S11694-021-00841-W

Soto, A., Ruiz, K.B., Ravaglia, D., Costa, G., Torrigiani, P., 2013. ABA may promote or delay peach fruit ripening through modulation of ripening- and hormone-related gene expression depending on the developmental stage. Plant Physiol. Biochem. 64, 11–24. https://doi.org/10.1016/j.plaphy.2012.12.011

Taiyun, W., Simko, V., 2021. R package "corrplot": visualization of a correlation.

Tanou, G., Minas, I.S., Scossa, F., Belghazi, M., Xanthopoulou, A., Ganopoulos, I., Madesis, P., Fernie, A., Molassiotis, A., 2017. Exploring priming responses involved in peach fruit acclimation to cold stress. Sci. Rep. 7, 1–14. https://doi.org/10.1038/s41598-017-11933-3

Tijero, V., Muñoz, P., Munné-Bosch, S., 2019. Melatonin as an inhibitor of sweet cherries ripening in orchard trees. Plant Physiol. Biochem. 140, 88–95. https://doi.org/10.1016/j.plaphy.2019.05.007

Tomás-Barberán, F.A., Gil, M.I., Cremin, P., Waterhouse, A.L., Hess-Pierce, B., Kader, A.A., 2001. HPLC−DAD−ESIMS analysis of phenolic compounds in nectarines, peaches, and plums. J. Agric. Food Chem. 49, 4748–4760. https://doi.org/10.1021/jf0104681

752 Tong, Z., Gao, Z., Wang, F., Zhou, J., Zhang, Z., 2009. Selection of reliable reference
753 genes for gene expression studies in peach using real-time PCR. BMC Mol. Biol.
754 10, 1–13. https://doi.org/10.1186/1471-2199-10-71

755 Tonutti, P., Casson, P., Ramina, A., 1991. Ethylene biosynthesis during peach fruit
756 development. J. Am. Soc. Hortic. Sci. 116, 274–279.
757 https://doi.org/10.21273/jashs.116.2.274

758 Tuan, P.A., Bai, S., Yaegaki, H., Tamura, T., Hihara, S., Moriguchi, T., Oda, K., 2015.
759 The crucial role of PpMYB10.1 in anthocyanin accumulation in peach and
760 relationships between its allelic type and skin color phenotype. BMC Plant Biol. 15,
761 1–14. https://doi.org/10.1186/s12870-015-0664-5

762 Wang, K., Shao, X., Gong, Y., Xu, F., Wang, H., 2014. Effects of postharvest hot air
763 treatment on gene expression associated with ascorbic acid metabolism in peach
764 fruit. Plant Mol. Biol. Report. 32, 881–887. https://doi.org/10.1007/s11105-014-
765 0699-z

766 Wang, X., Ding, Y., Wang, Y., Pan, L., Niu, L., Lu, Z., Cui, G., Zeng, W., Wang, Z.,
767 2017. Genes involved in ethylene signal transduction in peach (*Prunus persica*) and
768 their expression profiles during fruit maturation. Sci. Hortic. (Amsterdam). 224,
769 306–316. https://doi.org/10.1016/J.SCIENTA.2017.06.035

770 Zhang, X.M., Jia, H.J., 2005. Changes in aroma volatile compounds and ethylene
771 production during “Hujingmilu” peach (*Prunus persica* L.) fruit development. J.
772 plant Physiol. Mol. Biol. 31, 41–46.

773

774

FIGURES

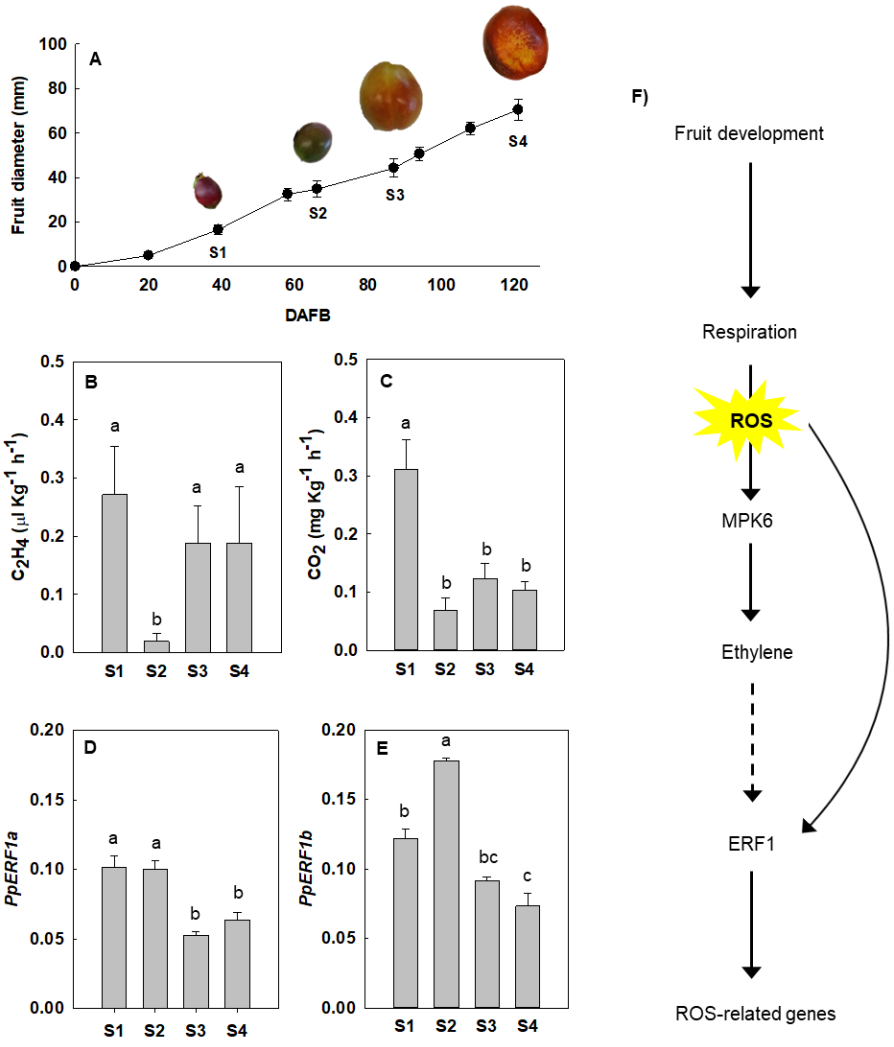

Figure 1. (A) Images of the different phenological stages of 'Diamond Ray' nectarines and fruit diameter (mm) monitored along the fruit development and ripening. (B) Ethylene production (µL Kg^{-1} h^{-1}) and (C) respiration rate (mg Kg^{-1} h^{-1}) of 'Diamond Ray' nectarines at each developmental stage. Gene expression analysis of (D) *PpERF1a* and (E) *PpERF1b* at each developmental stage. Error bars represent the standard errors of the means (n= 20 (A); n=4 (B-E)). Letters indicate significant differences ($p \leq 0.05$) between developmental stages. (F) Schematic representation of the ROS involvement in the activation of ROS-related genes through ERFs signaling (adapted from (Müller and Munné-Bosch, 2015).

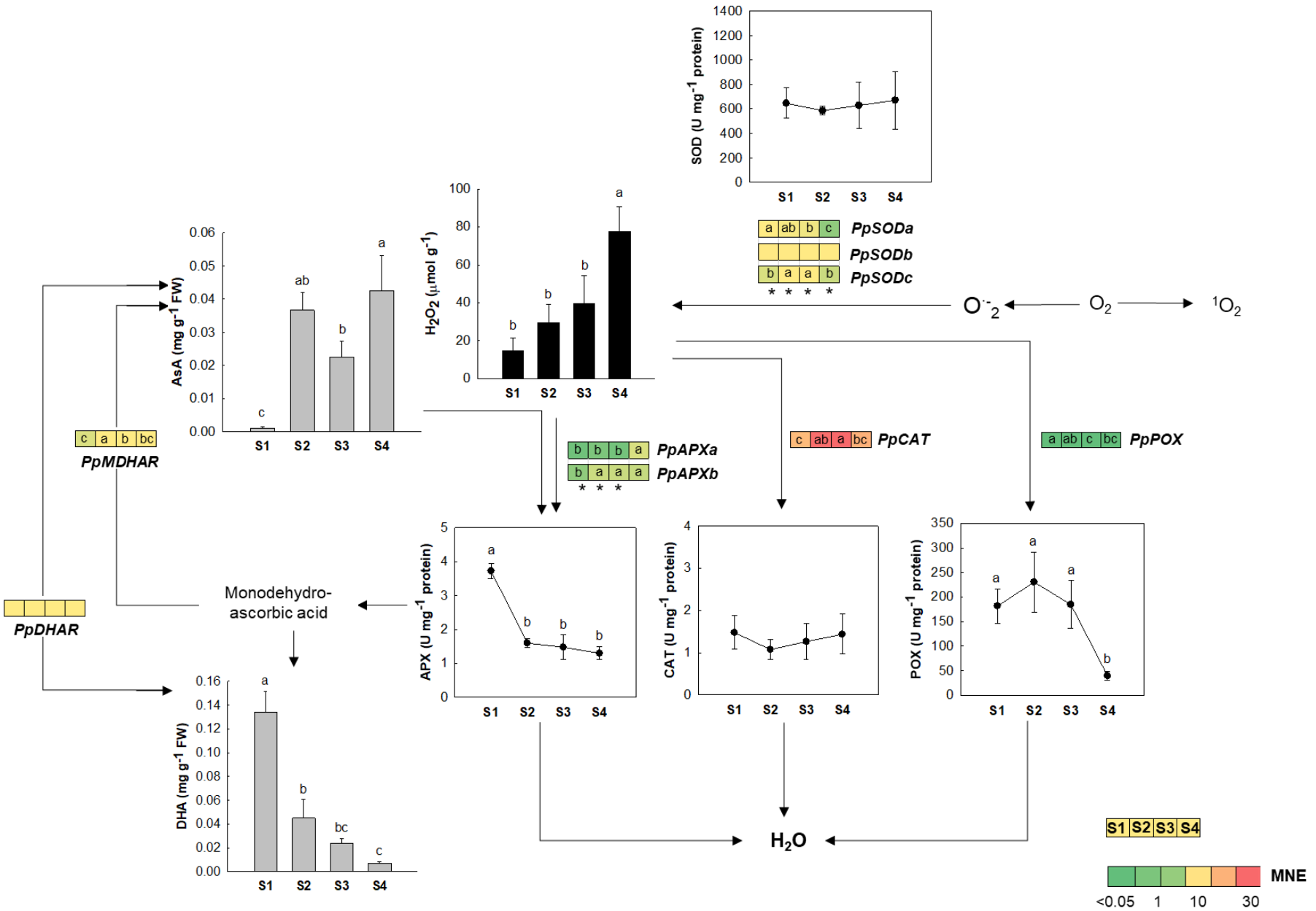
SOD (U mg-1 protein)
1400
1200
1000
800
600
400
200
0
S1 S2 S3 S4
a ab b c PpSODa
PpSODb
b a a b PpSODc
* * * *
O·-2
O2
1O2
H2O2 (μmol g-1)
100
80
60
40
20
0
a
b
b
b
AsA (mg g-1 FW)
0.06
0.05
0.04
0.03
0.02
0.01
0.00
c
ab
b
a
c a b bc PpMDHAR
b b b a PpAPXa
b a a a PpAPXb
* * *
c ab a bc PpCAT
a ab c bc PpPOX
PpDHAR
Monodehydro-
ascorbic acid
APX (U mg-1 protein)
5
4
3
2
1
0
a
b
b
b
CAT (U mg-1 protein)
4
3
2
1
0
POX (U mg-1 protein)
350
300
250
200
150
100
50
0
a
a
a
b
DHA (mg g-1 FW)
0.16
0.14
0.12
0.10
0.08
0.06
0.04
0.02
0.00
a
b
bc
c
H2O
S1 S2 S3 S4
MNE
<0.05 1 10 30

Figure 2. Overview of the ROS-scavenging metabolism and ascorbate pathway of 'Diamond Ray' nectarines during fruit development and ripening. The activity of the main antioxidant enzymes, as well as the content of ascorbic acid and H_2O_2 are represented in plots. The corresponding transcript levels of the main genes are represented as heatmaps. Different paralogs of the same gene are indicated as "a", "b" and "c". Error bars represent the standard errors of the means (n= 4). Letters indicate significant differences ($p \leq 0.05$) between developmental stages, while asterisk denote differences among paralogs at each developmental stage. (For interpretation of the references to colour in this figure legend, the reader is referred to the Web version of this article.)

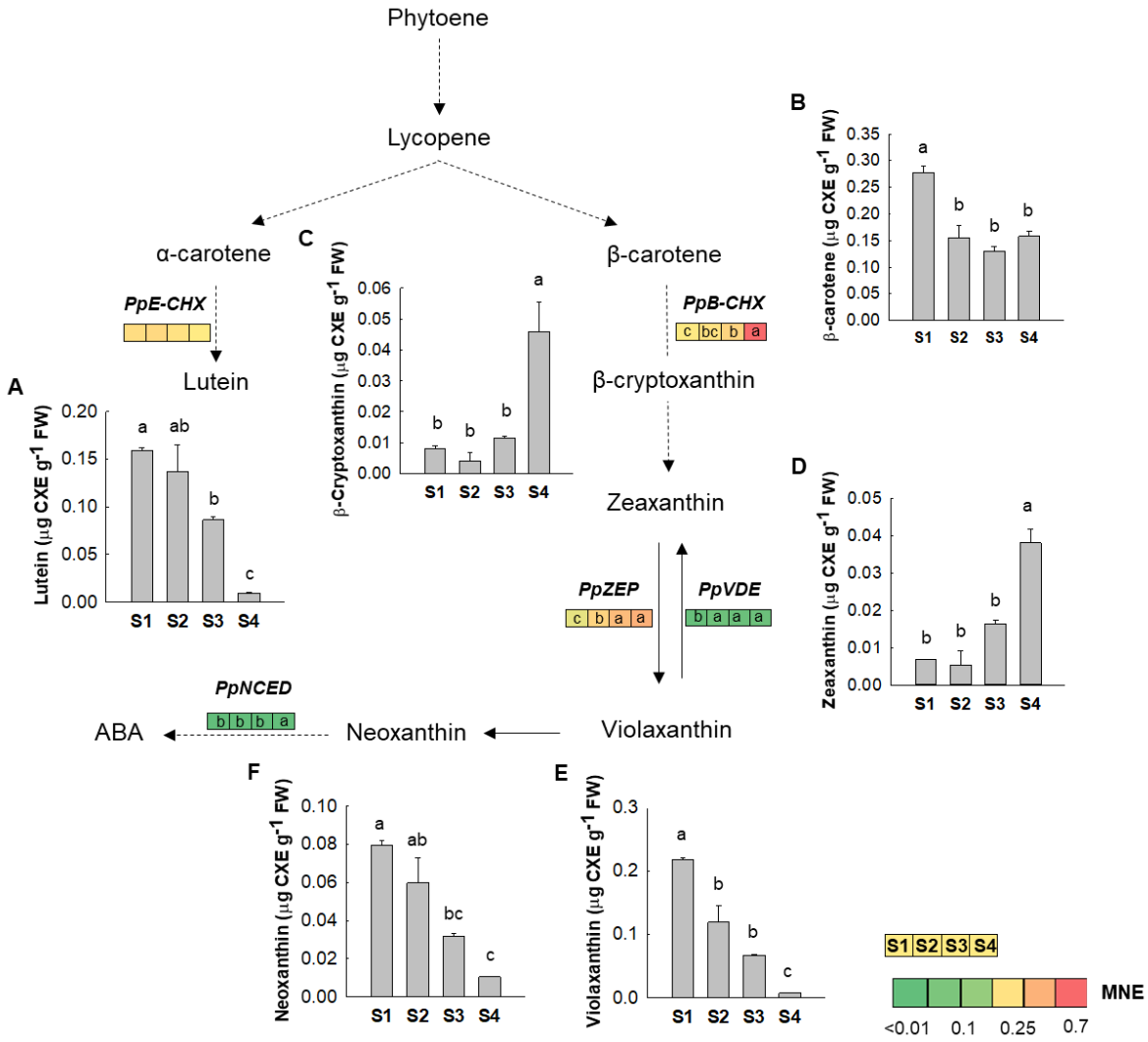

Figure 3. Carotenoid biosynthetic pathway of 'Diamond Ray' nectarines during fruit development and ripening. Carotenoid compounds are represented in plots, while the expression levels of the main genes are represented as heatmaps. The chemical composition of each compound is also indicated. Dashed lines indicate that some steps had been omitted. Error bars represent the standard errors of the means (n= 4). Letters indicate significant differences between ($p \leq 0.05$) developmental stages. (For interpretation of the references to colour in this figure legend, the reader is referred to the Web version of this article.)

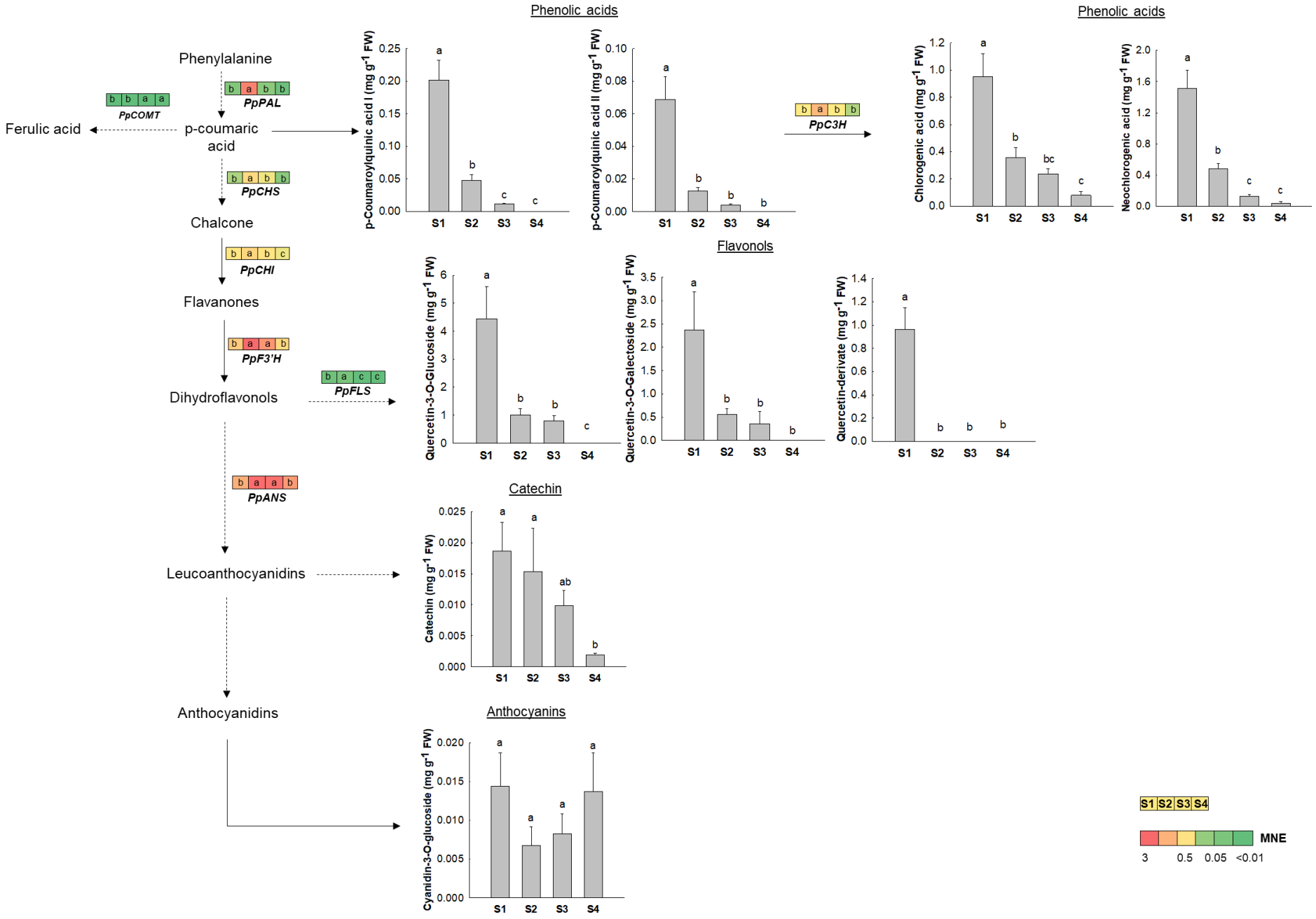
Phenylalanine
PpPAL
p-coumaric acid
PpCOMT
Ferulic acid
PpCHS
Chalcone
PpCHI
Flavanones
PpF3'H
Dihydroflavonols
PpFLS
PpANS
Leucoanthocyanidins
Anthocyanidins
PpC3H
Phenolic acids
p-Coumaroylquinic acid I (mg g-1 FW)
p-Coumaroylquinic acid II (mg g-1 FW)
Chlorogenic acid (mg g-1 FW)
Neochlorogenic acid (mg g-1 FW)
Flavonols
Quercetin-3-O-Glucoside (mg g-1 FW)
Quercetin-3-O-Galectoside (mg g-1 FW)
Quercetin-derivate (mg g-1 FW)
Catechin
Catechin (mg g-1 FW)
Anthocyanins
Cyanidin-3-O-glucoside (mg g-1 FW)
S1 S2 S3 S4
MNE
3 0.5 0.05 <0.01

Figure 4. Phenylpropanoid biosynthetic pathway of ‘Diamond Ray’ nectarines during fruit development and ripening. The different phenolic compounds identified are represented in plots, while the expression levels of the main genes are represented as heatmaps. Error bars represent the standard errors of the means (n= 4). Letters indicate significant differences between ($p \leq 0.05$) developmental stages. (For interpretation of the references to colour in this figure legend, the reader is referred to the Web version of this article.)

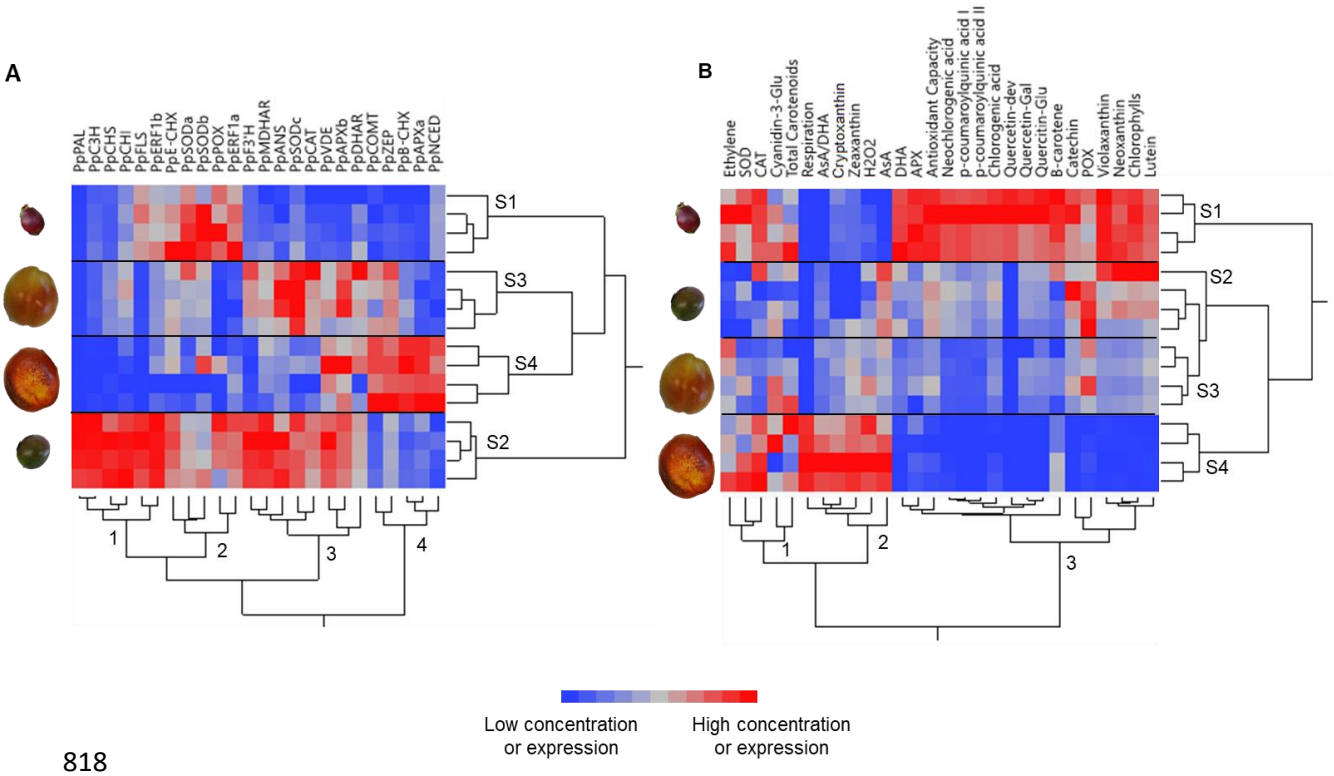

818

819

820 **Figure 5.** A two-way hierarchal cluster analysis (HCA) and heat map using gene
821 expression levels (A) and metabolite/enzyme activities (B) in four different stages (S1-
822 S4) along 'Diamond Ray' nectarine fruit development and ripening. Colours indicate the
823 relative concentration of each metabolite or the gene expression level, where red
824 represents high concentration or gene expression whereas blue depicts low concentration
825 or gene expression level. Columns indicate the different metabolites/enzymes activities
826 (A; n=28) or genes (B; n=24). Numbers indicated the different gene (A) or metabolite (B)
827 clusters generated within each hierarchical map. (For interpretation of the references to
828 colour in this figure legend, the reader is referred to the Web version of this article.)

829

830

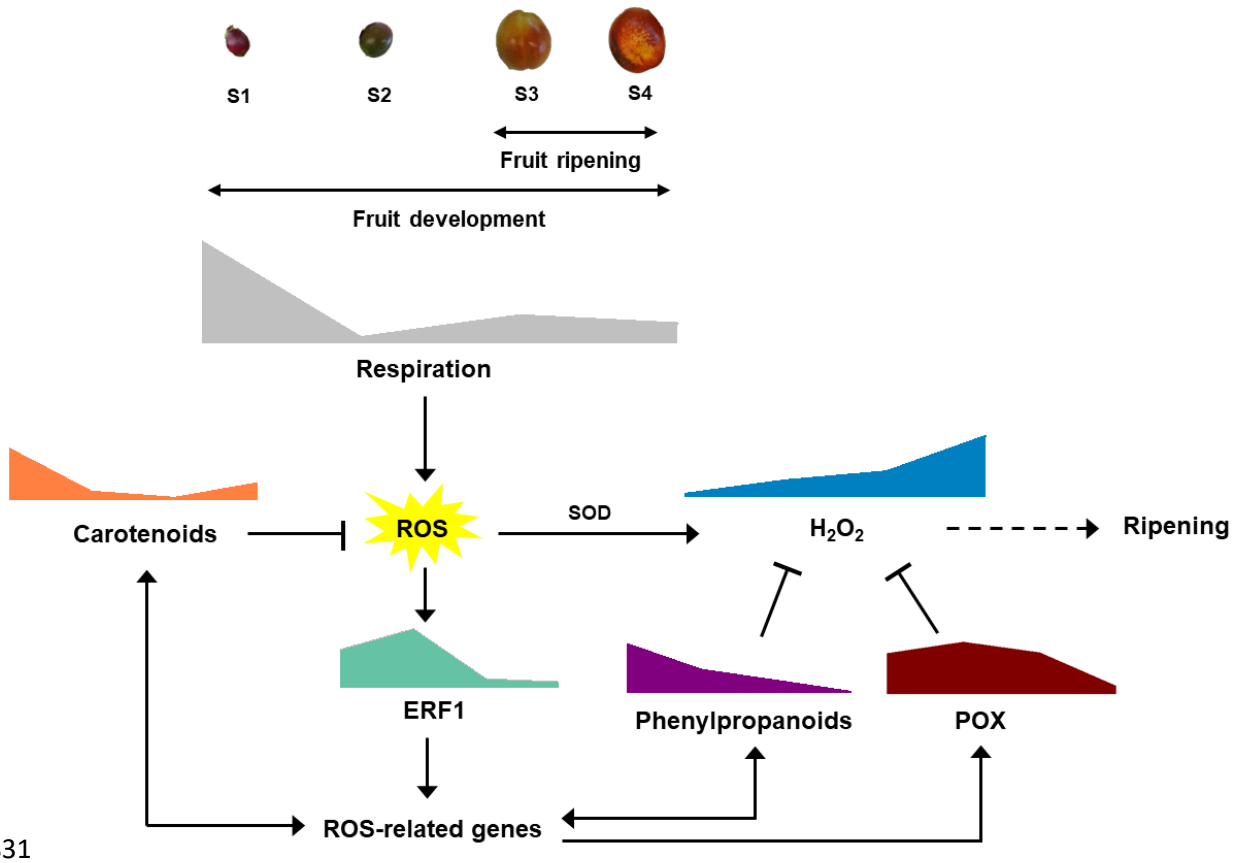

831

832 **Figure 6.** Schematic representation of the main events occurring during fruit development
833 and ripening of 'Diamond Ray' nectarines encompassing the four developmental stages
834 analysed in this study. Respiration rate, *ERF1* gene expression (the mean of both
835 *PpERF1a* and *PpERF1b*), total carotenoid, phenylpropanoid and H_2O_2 content, and POX
836 activity are included.

837

838

SUPPLEMENTARY TABLES

Supplementary Table 1. Real-time PCR primer set, including gene name and annotation, primer name and sequence, primer efficiency, metabolic pathway and/or gene function, localization, and primer source. Cellular localization was predicted by using the WoLF PSORT software (https://wolfpsort.hgc.jp/).

Gene	Annotation	Primer name	Primer sequence (5' – 3')	Efficiency	Metabolic pathway/function	Localization	Source
PpSODa	Superoxide dismutase	PpSODa-Fw PpSODa-Rv	GGATTATTCTCCGCTCCTTACTATTG CTCTCTTTTCTTCCTTTCTTCTGCTT	100 %	ROS-scavenging	Chloroplast	Huan et al., 2016
PpERF1a	Ethylene response factor 1a	PpERF1a-Fw PpERF1b-Rv	CTCCTCGGTGGCTGAACAT AGTGGCAGCAGACCCATA	95.69 %	ROS/ethylene-mediated signaling	Nucleus	Sherif et al., 2012
PpERF1b	Ethylene response factor 1b	PpERF1a-Fw PpERF1b-Rv	CGATTTCGGGTCCCATTT GCAAATCGCCCCAGTTTT	95.74 %	ROS/ethylene-mediated signaling	Nucleus	Sherif et al., 2012
PpSODb	Superoxide dismutase	PpSODb-Fw PpSODb-Rv	GTGGCTTTCAAACCTTCTCGCTTC CTGGTGGTGCTTCTGGTGATGGA	102.2 %	ROS-scavenging	Mitochondria	Huan et al., 2016
PpSODc	Superoxide dismutase	PpSODc-Fw PpSODc-Rv	CACGCAGGTGATTTGGGTAAC CAGATGACTTAAGGCCAATGATACC	103.3 %	ROS-scavenging	Cytoplasm	Huan et al., 2016
PpCAT	Catalase	PpCAT-Fw PpCAT-Rv	TCTCATACTGGTCTCAGGCAGATAAG CCACAAACACAAGCATACACACTAAG	97.4 %	ROS-scavenging	Peroxisome	Huan et al., 2016
PpPOX	Peroxidase	PpPOX-Fw PpPOX-Rv	GGTGTGGTGGAGCAAGCTCAAC GGGCAAACATTCTCGAGTGCAG	153.9 %	ROS-scavenging	Extracellular	Tanou et al., 2017
PpAPXa	Ascorbate peroxidase	PpAPXa-Fw PpAPXa-Rv	TATCAGAAGGCAGTGGAT GCTAATCGGAGAATTATAGGA	100.5 %	AsA-recycling pathway	Cytoplasm	Cao et al., 2017
PpAPXb	Ascorbate peroxidase	PpAPXb-Fw PpAPXb-Rv	GTAACATACGCAGACTTG CCATACTTCATAGGAATCTT	104. 6 %	AsA-recycling pathway	Chloroplast	Cao et al., 2017
PpMDHAR	Monodehydroascorbate reductase	PpMDHAR-Fw PpMDHAR-Rv	CCGGGTCATCGTTATAGGCT CATGAGGGCATCTAAACAGC	97.8 %	AsA-recycling pathway	Chloroplast	Wang et al., 2014
PpDHAR	Dehydroascorbate reductase	PpDHAR-Fw PpDHAR-Rv	GTTGGTGGACTTGGCTAA CAAAGGTGGATCTGGATACT	100.6 %	AsA-recycling pathway	Chloroplast	Cao et al., 2017
PpPAL	Phenylalanine ammonialyase	PpPAL-Fw PpPAL-Rv	AAGCTGCTGAAAAGGTGCAT TCATTTTGGTTGCTGCTCTG	102 %	Phenylpropanoid pathway	Cytoplasm	Jiao et al., 2014
PpC3H	p-coumarate 3-hydroxylase	PpC3H-Fw PpC3H-Rv	TCAGACTACTTCCGTTTGGAGCAG CAAGCCCTGGATTTTCCGAC	105.7 %	Phenylpropanoid pathway	Cytoplasm	Dardick et al., 2010
PpCOMT	Caffeic acid 3-O-methyltransferase	PpCOMT-Fw PpCOMT-Rv	CGCCTACGTGTGAAGAACGA TTGATGCGTGAGTAGCGAGT	95.6 %	Phenylpropanoid pathway	Cytoplasm	This study
PpCHS	Chalcone synthase	PpCHS-Fw PpCHS-Rv	AACCATCCTTCCCGACAGCGAT CAGAGATACCCAAAGGTTGGAAGGC	104.3 %	Phenylpropanoid pathway	Cytoplasm	Tuan et al., 2015
PpCHI	Chalcone isomerase	PpCHI-Fw PpCHI-Rv	ACACAGGTGACAACGATACTGCCACT TGAAGACCTCAAGGAACTTCTCAATGG	100.5 %	Phenylpropanoid pathway	Cytoplasm	Tuan et al., 2015
PpF3'H	Flavanone 3-hydroxylase	PpF3H-Fw PpF3H-Rv	TTGTGGAGGCTTGTGAGGATTGG TCCGAGGGCAGAGCGAAGAAC	99.6 %	Phenylpropanoid pathway	Cytoplasm	Tuan et al., 2015
PpFLS	Flavonol synthase	PpFLS-Fw PpFLS-Rv	GTTTTCTGACGGCAACGTTACGAA CCCAACCCTAGCGATAGGAGCC	98.2 %	Phenylpropanoid pathway	Cytoplasm	Ravaglia et al., 2013
PpANS	Anthocyanidin synthase	PpANS-Fw PpANS-Rv	GGAGTTGAAGAAGGCAGCAG GCCTGGTCATTGGCATACTT	100.3 %	Phenylpropanoid pathway	Cytoplasm	Tuan et al., 2015
PpB-CHX	Carotene β-hydroxylase	PpCHYB-Fw PpCHYB-Rv	GCTCGAGGAAGCTCTGTTTCA CTTGGGCTTTTTCTGTGCAATT	100.2 %	Carotenoid metabolism	Chloroplast	Brandi et al., 2011
PpE-CHX	Carotene ε-hydroxylase	PpCHYE-Fw PpCHYE-Rv	TCCAAGCATCCTTCGCTTTTT TCCAGCAACCAACATAGACAGAA	93.2 %	Carotenoid metabolism	Chloroplast	Brandi et al., 2011
PpZEP	Zeaxanthin epoxidase	PpZEP-Fw PpZEP-Rv	CCAAATATGGGTCAAGGTGGAT TTTCGCTACTTTTCTTCCATGCT	96.3 %	Carotenoid metabolism	Chloroplast	Brandi et al., 2011
PpVDE	Violaxanthin de-epoxidase	PpVDE-Fw PpVDE-Rv	AGTAGCTGGTTTGCTGGCAT TGGCAAGTTCTACCCTGCAT	103.6 %	Carotenoid metabolism	Chloroplast	This study
PpNCED1	9-cisepoxycarotenoid dioxygenase 1	PpNCED1-Fw PpNCED1-Rv	ATGGCTGCTCTTGGAAAAGC AGCCCATAGGATCCACTAGA	97.3 %	Carotenoid metabolism	Chloroplast	Brandi et al., 2011
PpTEF2	Translation elongation factor 2	PpTEF2-Fw PpTEF2-Rv	GGTGTGACGATGAAGAGTGATG TGAAGGAGAGGGAAGGTGAAAG	104.6 %	Reference gene		Tong et al., 2009

Supplementary Table 2. Individual phenolic compounds identified in 'Diamond Ray' nectarines, including chromatographic, spectroscopic, and spectrometric parameters.

Classification	Phenolic compound	λ_{max} (nm)	RT (min)	MS/MS cone voltage (V)	MS/MS collision energy (V)	$[M-H]^-$ molecular ion (m/z)	$[M-H]^-$ MS/MS daughter ions (m/z)
Phenolic acid	Neochlorogenic acid	326	6.8	25	25	353	191, 179, 135
Anthocyanin	Cyanidin 3-O-glucoside	515	7.7	-	-	-	-
Phenolic acid	p-Coumaroylquinic acid I	311	8.4	25	20	337	191, 173, 163
Phenolic acid	Chlorogenic acid	326	8.6	25	25	353	191
Flavan-3-ol	Catechin	280	9.0	25	25	289	109
Phenolic acid	p-Coumaroylquinic acid II	311	11.2	25	20	337	191, 173, 163
Flavonoid	Quercetin derivative	354	17.3	-	-	-	-
Flavonoid	Quercetin 3-O-galactoside	351	17.7	25	30	463	301
Flavonoid	Quercetin 3-O-glucoside	354	18.2	25	30	463	301

SUPPLEMENTARY FIGURES

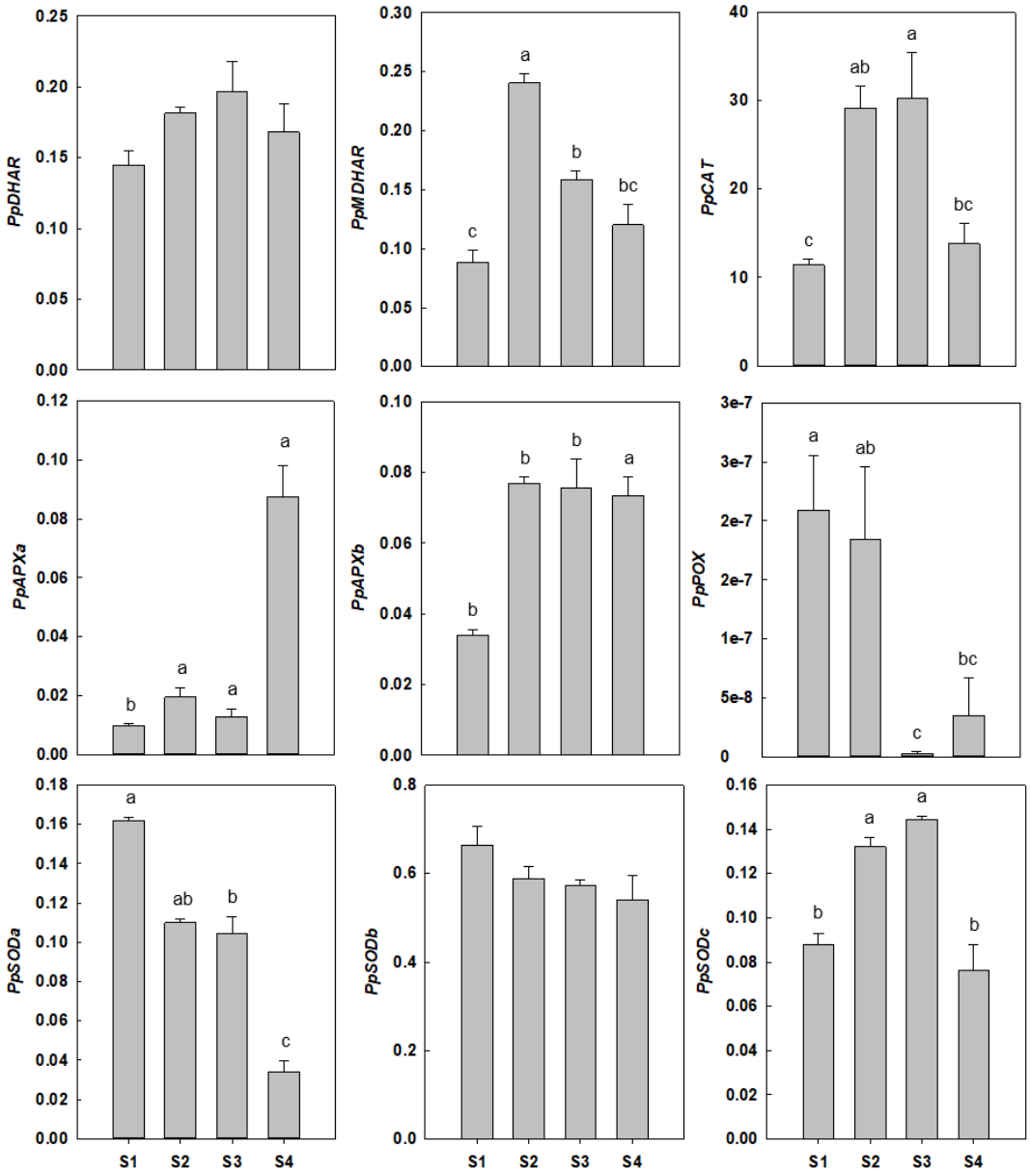

Supplementary Figure 1. Relative gene expression of antioxidant genes. Changes on relative gene expression of *PpSOD*, *PpAPX*, *PpCAT*, *PpPOX*, *PpMDHAR* and *PpDHAR* genes at the different developmental stages of 'Diamond Ray' nectarines. Different paralogs are indicated as "a", "b" and "c". Each point represents the mean of 4 biological replicates and vertical bars indicate the standard error of the mean. Different letters indicate significant differences between developmental stages ($p \leq 0.05$).

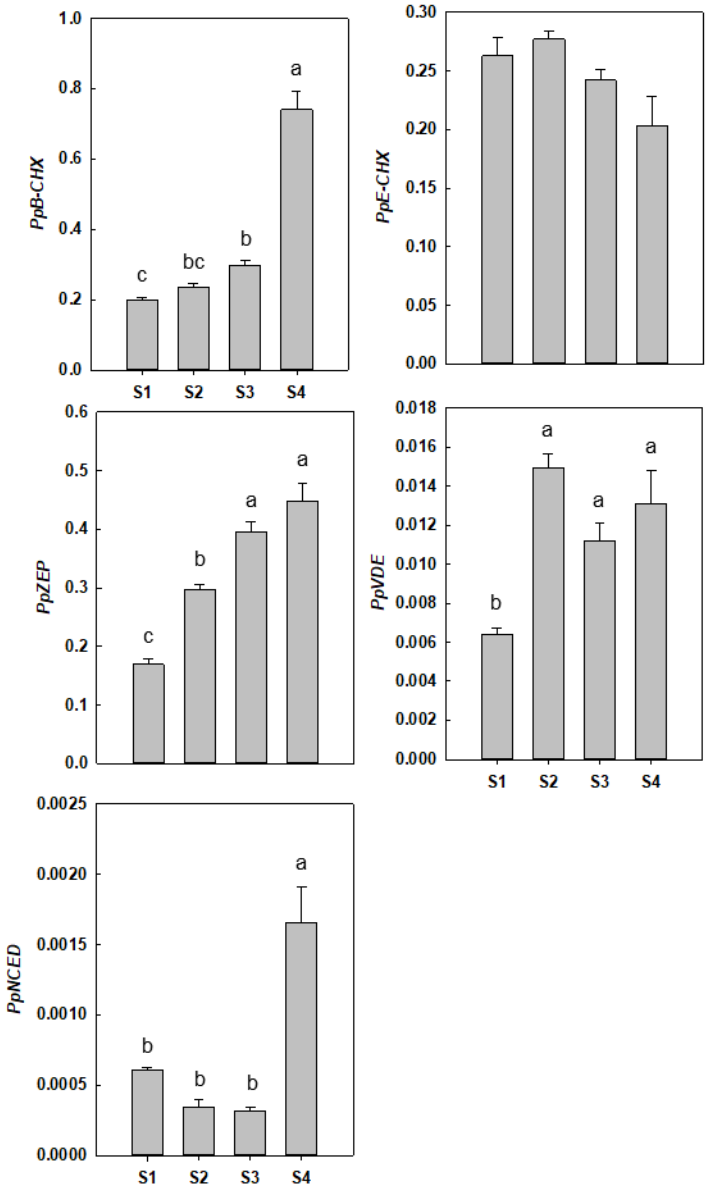

855

856 **Supplementary Figure 2. Relative gene expression of carotenoid biosynthetic genes.**

857 Changes on relative gene expression of *PpB-CHX*, *PpE-CHX*, *PpZEP*, *PpVDE* and

858 *PpNCED* genes at the different developmental stages of 'Diamond Ray' nectarines. Each

859 point represents the mean of 4 biological replicates and vertical bars indicate the standard

860 error of the mean. Different letters indicate significant differences between

861 developmental stages ($p \leq 0.05$).

862

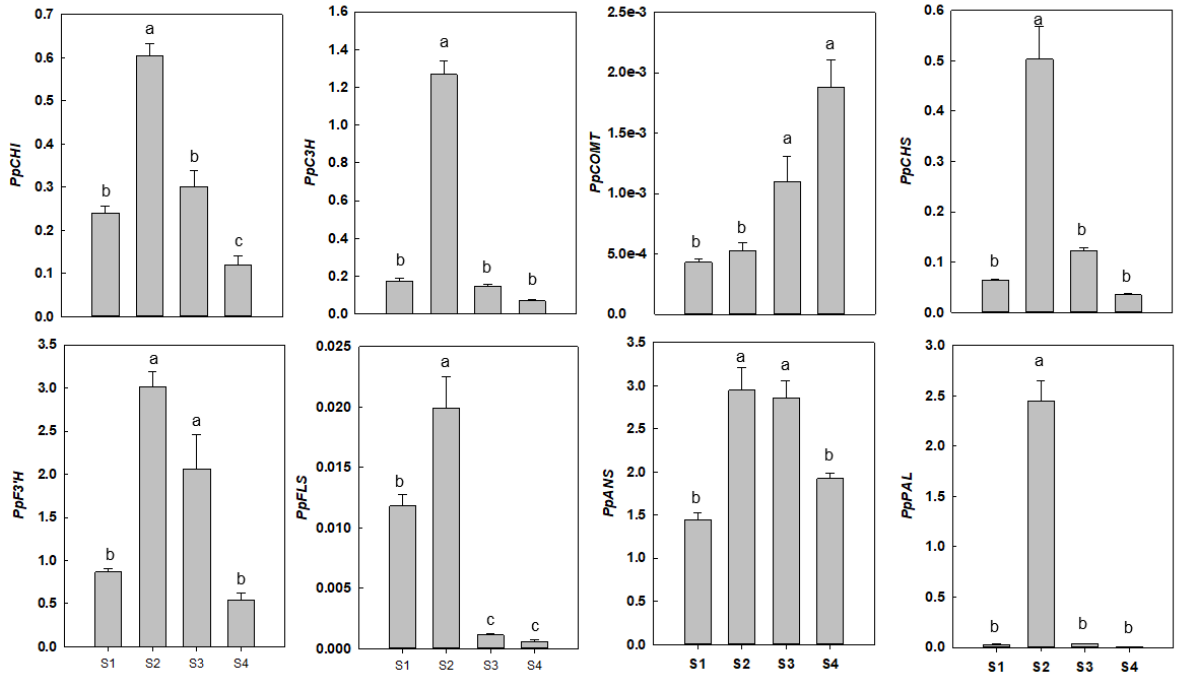

Supplementary Figure 3. Relative gene expression of phenylpropanoid-related genes. Changes on relative gene expression of *PpPAL*, *PpCOMT*, *PpC3H*, *PpCHS*, *PpCHI*, *PpF3'H*, *PpFLS* and *PpANS* genes at the different developmental stages of 'Diamond Ray' nectarines. Each point represents the mean of 4 biological replicates and vertical bars indicate the standard error of the mean. Different letters indicate significant differences between developmental stages ($p \leq 0.05$).

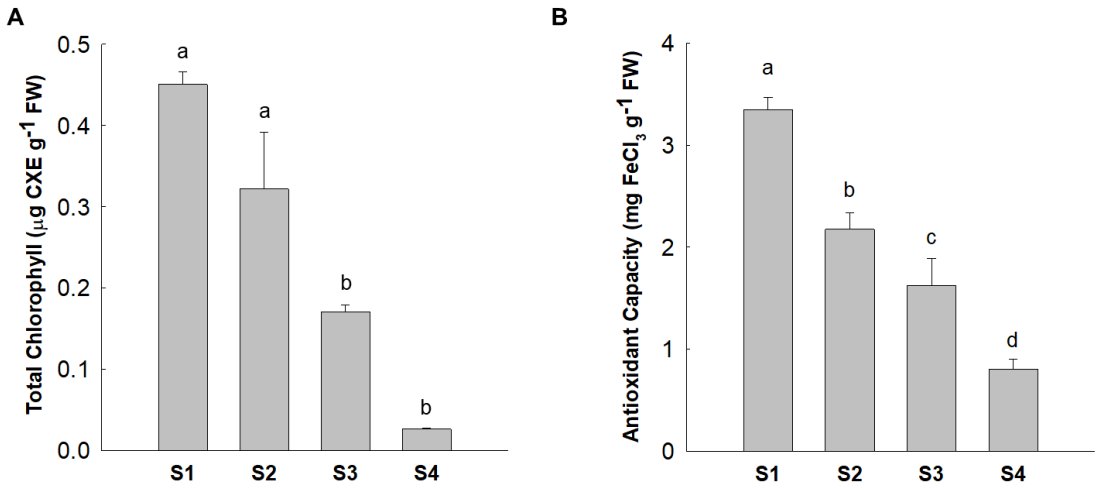

871

872 **Supplementary Figure 4.** (A) Total chlorophyll content and (B) antioxidant capacity
873 during the development and ripening of 'Diamond Ray' nectarines. Each point represents
874 the mean of 4 biological replicates and vertical bars indicate the standard error of the
875 mean. Different letters indicate significant differences between developmental stages ($p \leq$
876 0.05).

877

878

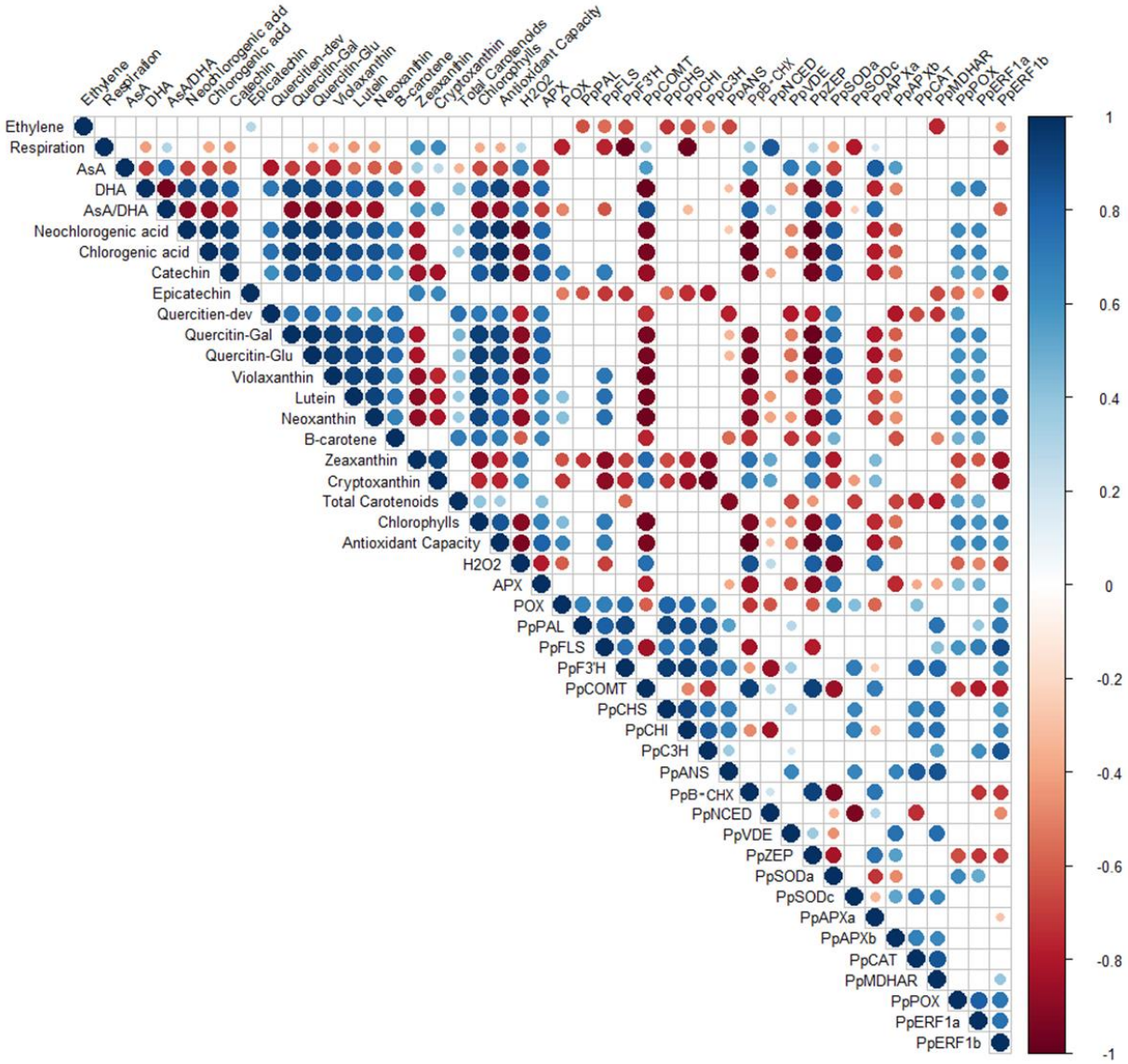

879

880 **Supplementary Figure 5.** Bivariate correlations among the different parameters
881 (including respiration, ethylene, enzymes, metabolites and genes) analysed during the
882 development and ripening of 'Diamond Ray' nectarines. The size of the circle for each
883 correlation and the colour depict the significance and the correlation coefficient,
884 respectively. Positive correlations coefficients are displayed in blue and negative
885 correlations coefficients in red.